

# Adaptive dynamics of eco-evolutionary repeated games: Effect of reward and punishment

Prosanta Mandal,<sup>1,\*</sup> Suman Chakraborty,<sup>2,†</sup> Vaibhav Madhok,<sup>2,‡</sup> and Sagar Chakraborty<sup>1,§</sup>

<sup>1</sup>*Department of Physics, Indian Institute of Technology Kanpur, Kanpur, Uttar Pradesh, PIN: 208016, India*

<sup>2</sup>*Department of Physics, Indian Institute of Technology Madras, Chennai 600036, India*

Long-term evolutionary processes can strongly influence common-pool resource conservation by generating new traits or behaviours that modify the feedback between population strategies and the resource state. Here we develop an eco-evolutionary framework in which individuals repeatedly interact with the same opponent and follow direct reciprocity through reactive strategies. The strategic dynamics is coupled to a renewable common resource and analyzed using adaptive dynamics. After our exhaustive non-linear dynamical analysis of  $2 \times 2$  strategic games, we focus on comparative and combined usefulness of institutional incentives in the form of rewards and punishments in preventing the Tragedy of the Commons even when defection dominates in the replete resource state. We also report possibility of robust stable oscillations—emerging via Hopf bifurcation—in resource state and population strategies.

## I. INTRODUCTION

The Tragedy of the Commons (ToC) [1–6] refers to a social dilemma in which individuals, acting in their self-interest, overuse and ultimately deplete shared resources, resulting in collective harm. This phenomenon arises across diverse domains, including population growth [1], environmental degradation [7–10], property and communal rights [11], wildlife crimes [12, 13], and even plant competition [14]. The pivotal concern lies in designing mechanisms that manage common resources effectively, balancing individual incentives with long-term collective sustainability.

While one would naturally guess that cooperation in a society would prevent the ToC, there remains a fundamental puzzle in evolutionary biology and game theory about how cooperation can emerge and persist among selfish individuals. The Donation Game (DG)—a variant of the Prisoner’s Dilemma (PD)—offers a minimal yet powerful framework for studying this question [15, 16]. In this game, one individual pays a cost to confer a benefit to another. Mutual cooperation results in a socially optimal outcome, yet individuals are often tempted to defect and enjoy the benefits without incurring the cost. The tension between individually rational strategies and collectively desirable outcomes encapsulates a deep evolutionary paradox: if natural selection favours selfishness, why is cooperation so prevalent in nature and society? Numerous works have been done in this direction and ‘five rules of cooperation’ [17] (which includes direct reciprocity [18–21]—focus of this paper) notably summarizes many of them within the paradigm of evolutionary game theory [22–25].

Environmental variability plays a crucial role in shaping cooperation and social behaviour. Organisms constantly adapt to fluctuations in climate, resources, and habitat conditions [26–28]. A classic example is the peppered moth during the Industrial Revolution, where changes in tree coloration shifted selective advantages between morphs [29]. Seasonal scarcity

can intensify competition, alter social hierarchies, or trigger new cooperative strategies [18]. Predator-prey dynamics, for instance, evolve with shifting environmental conditions, as prey adopt new defences and predators adjust tactics [30]. These adaptations ripple through ecological networks, reshaping interactions and enabling the emergence of symbioses [31], behavioral innovation [32], and even speciation events [33–40].

Empirical examples of eco-evolutionary feedbacks include algae–rotifer chemostats [41], alewife–zooplankton dynamics in North American lakes [42–44], guppies in Trinidadian streams [45, 46], Darwin’s finches in the Galápagos [47–49], and poplar trees in North America [50]. These systems highlight how behavioural strategies and environmental context co-evolve, forming dynamic feedback loops.

Evidently, in an ecosystem, biotic interactions—such as competition, predation, and cooperation—are not isolated from the abiotic environment, including climate, temperature, and resource availability. These biotic and abiotic components are inherently coupled, meaning changes in one can influence the dynamics of the other. For instance, climate change (an abiotic shift) can alter species interactions, migration patterns, or reproductive strategies. In contrast, widespread changes in population behaviour can, in turn, affect nutrient cycling, atmospheric composition, or habitat structure. To study such coupled dynamics, researchers often model the environment using two distinct states or regimes—commonly representing different levels of common-pool resources [51–58]; while the cooperative interaction between the agents is modelled as one-shot games with no memory of what opponents did to them in the past.

However, to the best of our knowledge, all such theoretical research directions completely ignored the natural reaction of agents to opponent’s past actions. Also, the evolutionary dynamics studied has usually been short-term replicator dynamics [25, 59–63] while ignoring the long-term evolutionary implications of game-environment feedback. In this paper, we focus on direct reciprocity—tendency of individuals strategize in reaction to their opponents’ actions—which fosters cooperative behaviour deciding a resource’s fate; and investigate how the feedback of this resource state on the strategies further impacts the ToC. To this end, we adopt the formalism of

\* [prosantam21@iitk.ac.in](mailto:prosantam21@iitk.ac.in)

† [ph25r001@mail.iitm.ac.in](mailto:ph25r001@mail.iitm.ac.in) (Corresponding author)

‡ [madhok@physics.iitm.ac.in](mailto:madhok@physics.iitm.ac.in)

§ [sagarc@iitk.ac.in](mailto:sagarc@iitk.ac.in)

repeated games [19, 64, 65] among agents endowed with reactive strategies [23, 64, 66]; and the long-term evolutionary dynamics is modelled using the adaptive dynamics [25, 32, 67–70].

Additionally, after having presented the general framework of ‘adaptive dynamics of eco-evolutionary repeated games’, we study the effects of institutional incentives—like rewards and punishments—on this game-environment feedback or eco-evolutionary dynamics.

It is well-known that across the natural world, from microbial symbioses to complex human societies, cooperation is often sustained through mechanisms of reward and punishment. For example, in the cleaner fish mutualism [71], the cleaner fish *Labroides dimidiatus* benefits by eating ectoparasites off client reef fish. When it cheats by feeding on protective mucus instead, clients punish it by fleeing or switching partners. In the legume–rhizobium mutualism [72], plants sanction ineffective rhizobia by limiting oxygen supply and reducing nodule size. Similarly, in mycorrhizal associations [73], plants preferentially reward fungal hyphae that deliver more nutrients with greater carbon allocation. In human societies also, prosocial behaviour is promoted through reward and punishment [74–76]. Individuals may even incur personal costs to punish defectors or free-riders, sustaining cooperation through altruistic or norm-enforcing behavior. Such mechanisms are central to understanding the evolution and maintenance of cooperation.

In evolutionary public goods games (PGG), both reward and punishment can foster cooperation [77–79]. Punishment enhances cooperation via altruistic enforcement, reciprocity, or exclusion [74, 75, 80, 81]. Targeted punishment, in particular, can transform a defector-dominated population into one of global cooperation through feedback loops [82–84]. However, punishment alone may be insufficient or inefficient in maintaining cooperative equilibria, especially under environmental or strategic uncertainty.

A growing body of work has explored how the interplay of reward and punishment shapes social outcomes. Studies have examined their relative importance [55, 85], roles in second-order punishment and indirect reciprocity [86], and potential for addressing large-scale coordination challenges like climate change [87]. In engineered systems, reward-punishment mechanisms have been proposed to regulate unwanted network traffic by incentivizing cooperation [88]. Other work has modelled third-party interventions, showing that the combined use of reward and punishment achieves faster and more robust cooperation than either strategy alone [89]. Moreover, in peer-based PGGs, reward was found to facilitate mutual benefit in localized groups, though its role in large-scale cooperation was more limited [90].

Despite this growing understanding, in the context of this paper an obvious lacuna gap remains: what is the interplay of reward and punishment in promoting cooperation under long-term adaptive dynamics of eco-evolutionary game dynamics? To the best of our knowledge, the literature lacks a clear demarcation of the maximal effectiveness of reward and punishment in reactive strategy spaces. To this end, in Sec. II, we introduce the mathematical framework, and present the generic

results in Sec. III. Subsequently, in the light of those results, we understand the effects of reward and punishment in Sec. IV before concluding in Sec. V.

## II. THE MODEL

Consider a large (mathematically, infinite) unstructured population with access to a common resource. The individuals are randomly paired to allow them play a two-action–two-player game repeated infinitely using reactive (also called memory-half) strategies where each player consider only her opponent’s most recent action. The reactive strategies are specified as a 3-tuple [23, 25, 66, 91, 92],  $E = (y, p, q)$ , where the player with the strategy  $E$  starts the repeated game with the action C (to cooperate) with probability  $y$  or with action D (to defect) with probability  $1 - y$ ; furthermore, in every subsequent round of play, the player reciprocates with action C with probability  $p$  (or action D with probability  $1 - p$ ) if her opponent cooperated in the immediately preceding round and reciprocates with action C with probability  $q$  (or action D with probability  $1 - q$ ) if her opponent defected in the immediately preceding round. In this paper, we confine our interest to the cases where  $y$ ,  $p$ , and  $q$  lie between zero to one. This renders the strategy space to be effectively an open unit square where each point is a strategy denoted by the coordinate,  $(p, q)$ . It is well-known that when a player with strategy  $(p, q)$  plays with another player with strategy  $(p', q')$ , the  $m^{\text{th}}$ -level cooperation levels  $C_m$  and  $C'_m$  of the two player, respectively, asymptotically converges to

$$C = \frac{q + rq'}{1 - rr'} \quad \text{and} \quad C' = \frac{q' + r'q}{1 - rr'}, \quad (1)$$

where  $r \equiv p - q$  and  $r' \equiv p' - q'$ .

As is customary in the literature of eco-evolutionary games where game-environment feedback is taken into account, the effect of state of the resource is incorporated in the payoff matrix as follows [51]

$$\Pi \equiv \begin{bmatrix} R & S \\ T & P \end{bmatrix} \equiv (1 - n) \begin{bmatrix} R_0 & S_0 \\ T_0 & P_0 \end{bmatrix} + n \begin{bmatrix} R_1 & S_1 \\ T_1 & P_1 \end{bmatrix}, \quad (2)$$

where the state of the resource,  $n$ , is normalized to range from zero to one. Essentially, one is accounting for the fact the payoff matrix, and hence the equilibrium action of the players, can change with the resource-state. Here, the first row and the second row correspond to the focal player’s action C and D, respectively; while the first column and the second column correspond to the opponent player’s action C and D, respectively. With this payoff matrix in mind, after infinitely many repeated interactions, the average payoff of the focal player can easily be shown to be [91],

$$A = (\beta - \gamma)C'C - \beta C' + (\alpha + \gamma)C + P, \quad (3)$$

where,  $\gamma \equiv T - R$ ,  $\beta \equiv P - S$  and  $\alpha \equiv R - P$ .

Our focus is on the long-term evolutionary dynamics which occurs in the mutation-selection dominated regime which is

conveniently studied through the theoretical framework of adaptive dynamics [25, 66]. It considers the continuous evolution of strategies in response to small mutations and the resulting fitness landscape. Specifically, one considers strategy-wise homogeneous population where only a single mutant arises at any given instant, and it is either driven to extinction or fixed in the population before the appearance of the next mutant. If the mutant strategy is nearly identical to that of the resident, then the discrete-step substitution sequence can be approximated by the continuous trajectory of adaptive evolution in trait space [91, 93, 94] (i.e.,  $p$ - $q$  space in our context).

To formalize the framework, one defines the relative fitness  $S(E', E)$ , also known as invasion fitness [95] of a mutant against resident:

$$S(E', E) = A(E', E) - A(E, E). \quad (4)$$

Hence, the dynamical equations in  $p$ - $q$  space can be obtained as

$$\dot{p} = \frac{\partial S}{\partial p'} \Big|_{\substack{p'=p \\ q'=q}} = \frac{q}{(1-r^2)(1-r)^2} F(p, q, n), \quad (5a)$$

$$\dot{q} = \frac{\partial S}{\partial q'} \Big|_{\substack{p'=p \\ q'=q}} = \frac{(1-p)}{(1-r^2)(1-r)^2} F(p, q, n). \quad (5b)$$

Here,

$$F(p, q, n) \equiv (1-n) [(\beta_0 - \gamma_0)q(1+r) + (\alpha_0 + \gamma_0)r(1-r) - \beta_0(1-r)] + n [(\beta_1 - \gamma_1)q(1+r) + (\alpha_1 + \gamma_1)r(1-r) - \beta_1(1-r)], \quad (6)$$

where  $\gamma_0 \equiv T_0 - R_0$ ,  $\beta_0 \equiv P_0 - S_0$ ,  $\alpha_0 \equiv R_0 - P_0$ ,  $\gamma_1 \equiv T_1 - R_1$ ,  $\beta_1 \equiv P_1 - S_1$ , and  $\alpha_1 \equiv R_1 - P_1$ .

It is easily realized that the invasion of a mutant strategy can influence the state of common resource, which in turn can modulate the fitness landscape of the population. If we consider that the resource undergoes a logistic growth such that its growth is sustained by the propensity of cooperation in the population (while the defectors only degrade the resource), then its dynamics as the form

$$\dot{n} = \varepsilon n(1-n)f(p, q). \quad (7)$$

Here,  $\varepsilon$  (a positive real number) characterized the relative speed of the resource-state dynamics compared to that of the traits' and  $f(p, q)$  may be modelled in two different ways: In one approach, we consider the state of the resource to be dependent on the players' trait values (i.e., their conditional probabilities of cooperating or defecting), while the second approach links the state of the resource to the asymptotic cooperation level.

Thus, in the first approach, one may define a simple form  $f(p, q) = [\theta \cdot p - (1-p)] + [\theta \cdot q - (1-q)]$  so that the feedback of reciprocity ( $p$ ) and generosity ( $q$ ) traits on the resource is rather direct. The positive parameter  $\varepsilon$  represents the relative rate (compared to the adaptive dynamics) with which individual trait frequencies modify the resource state. The positive

parameter  $\theta$  is the ratio of the enhancement rate to degradation rate due to adoption of actions C and D. Alternatively, as the other approach, one could define  $f(p, q) = \theta \cdot C - (1-C)$  where growth rate is effected by the asymptotic cooperation level (a robust measure of propensity of cooperation in the population) and the decay rate is effected by the asymptotic defection level.

Interestingly, when  $\theta = 1$ , i.e., the cooperators and the defectors impact the resource symmetrically, the two forms of  $f(p, q)$  are same except for a positive multiplicative factor,  $\frac{1}{2(1-r)}$ . This leads to unchanged conclusions about the existence of fixed points and their nature of stability in  $p$ - $q$ - $n$  dynamics. Moreover, the dynamical outcomes of the strategy-resource remains qualitatively unchanged for all values of  $\varepsilon$ . Thus, henceforth we set  $\theta = 1$  and  $\varepsilon = 1/2$  to arrive at the following simple form of the resource dynamics:

$$\dot{n} = n(1-n) [(p+q) - 1]. \quad (8)$$

### III. LINEAR STABILITY ANALYSIS

The  $p$ - $q$ - $n$  dynamics is, thus, governed by Eqs. (5) and (8). We now perform its stability analysis.

#### A. Fixed points and saturated boundary points

First we note that for this system with free parameters  $\alpha_0, \alpha_1, \beta_0, \beta_1, \gamma_0$  and  $\gamma_1$ , there are six different types of sets of phase points of interest. Three of them are sets of non-isolated fixed points:

- (i) non-isolated fixed points at the intersection of surfaces— $n = 0$  and  $F(p, q, n) = 0$  (see Fig. 1(A)) and Appendix A for the stability property of these fixed points),
- (ii) non-isolated fixed points at the intersection of surfaces— $n = 1$  and  $F(p, q, n) = 0$  (see Fig. 1(B)) and Appendix B to get the stability property of these fixed points),
- (iii) non-isolated fixed points at the intersection of surfaces— $p + q = 1$  and  $F(p, q, n) = 0$  (see Fig. 1(C)) and Appendix C to get the stability property of these fixed points).

Remaining two are saturated points [16]:

- (iv) (strictly) saturated boundary points— $(p, q, n) = (p, 0, 0)$ ,
- (v) (strictly) saturated boundary points— $(p, q, n) = (1, q, 1)$ .

Note that nature of these points requires that the closure of the open reactive strategy space be considered in order to investigate the saturation behaviour in the limiting region approaching the boundary: The saturated boundary points lies

on the boundary of the closure of phase space. In this context we recall that on the boundary of  $[0, 1]^3$  (i.e., set of all points  $(p, q, n) \in [0, 1]^3$ )—the unit phase cube—such that exactly one coordinate equals to 0 or 1) a point is (strictly) saturated if the phase velocity at that point tends to push it out of the unit phase cube; in other words, a strictly saturated boundary point is the  $\omega$ -limit of some phase trajectory emanating in the interior.

First consider the possibility of saturated boundary points at  $n = 0$  plane. The condition to reach the  $n = 0$  plane is  $\dot{n} < 0$  which implies the following constraints on the possible reactive strategies  $p + q < 1$  (see Eq. 8). Therefore, at  $n = 0$  plane, the trajectories cannot reach  $p = 1$  and  $q = 1$ . A glance at Eq. 5 further suggests at  $q = 0$  with  $F(p, q, n = 0) < 0$ ,  $\dot{q} < 0$  (and  $p$  does not change). Thus, points  $(p, q, n) = (p, 0, 0)$  tend to get pushed out away from the phase space; and thus, qualify as saturated boundary points. The condition for those to exist is: if  $\alpha_0 + \gamma_0 > 0$ , then  $p < \frac{\beta_0}{\alpha_0 + \gamma_0}$ ; if  $\alpha_0 + \gamma_0 < 0$ , then  $p > \frac{\beta_0}{\alpha_0 + \gamma_0}$ ; and if  $\alpha_0 + \gamma_0 = 0$ , it follows that  $\beta_0 > 0$  for any  $p$  (see Eq. 6).

Similarly, saturated boundary points can also appear at  $n = 1$  plane. In this case the condition for a trajectory to reach the  $n = 1$  plane is  $p + q > 1$  (see Eq. 8); the trajectories cannot reach  $p = 0$  and  $q = 0$ . Again inspection of Eq. 5 suggests at  $p = 1$  with  $F(p, q, n = 0) > 0$ ,  $\dot{p} > 0$  (and  $q$  does not change). Thus,  $(p, q, n) = (1, q, 1)$  are saturated boundary points which tend to get pushed out away from the phase space. The condition for them to exist is:  $\frac{\alpha_1 + \beta_1 - \gamma_1}{(\alpha_1 + \beta_1)} > q$  if  $\alpha_1 + \beta_1 > 0$ ;  $\frac{\alpha_1 + \beta_1 - \gamma_1}{(\alpha_1 + \beta_1)} < q$  if  $\alpha_1 + \beta_1 > 0$ ; and if  $\alpha_1 + \beta_1 = 0$ , it follows that  $\gamma_1 > 0$  for any  $q$  (see Eq. 6).

## B. Limit cycle via Hopf bifurcation

Besides the equilibrium evolutionary outcomes, there may be a possibility of periodically oscillating evolutionary outcomes which would correspond to existence of limit cycles. Emergence of the Hopf bifurcation [96], in particular, marks a critical transition where a fixed point changes its nature of stability leading to limit cycle oscillations as system parameters vary. In our framework, a Hopf bifurcation can arise only around the internal fixed points of type (iii). One of the three eigenvalues (see Appendix C) at this internal non-isolated fixed points always possesses zero, reflecting the neutral direction along the fixed points. The remaining two eigenvalue ( $\lambda_1$  and  $\lambda_2$ ) determine the local stability in the transverse directions of the fixed points:

$$\lambda_1 = \frac{L - \sqrt{L^2 - 4\eta}}{2} \text{ and } \lambda_2 = \frac{L + \sqrt{L^2 - 4\eta}}{2}, \quad (9)$$

where,

$$\eta = \frac{n(1-n)}{4pq} \frac{(\beta_1 + \gamma_1)\alpha_0 - (\beta_0 + \gamma_0)\alpha_1}{(1-n)(\beta_0 + \gamma_0 + 2\alpha_0) + n(\beta_1 + \gamma_1 + 2\alpha_1)}, \quad (10a)$$

$$L = \frac{1}{4q} [(\beta_0 - \gamma_0)(1-n) + (\beta_1 - \gamma_1)n]. \quad (10b)$$

A Hopf bifurcation can occur when the two non-zero eigenvalues  $\lambda_1$  and  $\lambda_2$  form a complex conjugate pair whose real part changes sign from negative to positive, thereby giving rise to a small-amplitude stable limit cycle emerging from a previously stable internal fixed point. The discriminant of the term inside the square root of Eq. (9) must be negative. In our setting, the Hopf bifurcation occurs at  $L = 0$ , where the real part of the eigenvalues vanishes. This condition ultimately reduces to the following requirement on the resource:

$$n = \hat{n} \equiv \frac{\beta_0 - \gamma_0}{(\beta_0 - \gamma_0) - (\beta_1 - \gamma_1)}. \quad (11)$$

Inspection of Eq. (11) shows that  $\hat{n} \in [0, 1]$  only for one of the following mutually exclusive parametric configurations: (i)  $\beta_0 \geq \gamma_0$  and  $\beta_1 \leq \gamma_1$  or (ii)  $\beta_0 \leq \gamma_0$  and  $\beta_1 \geq \gamma_1$ . Now, for a Hopf bifurcation to occur at  $n = \hat{n}$ ,  $\eta$  has to be positive; only then eigenvalues  $\lambda_1$  and  $\lambda_2$  become purely imaginary. On inspecting the numerator and denominator of RHS in Eq. (10a), this is found to occur when either  $(\beta_1 + \gamma_1)\alpha_0 > (\beta_0 + \gamma_0)\alpha_1$  and  $(1 - \hat{n})(\beta_0 + \gamma_0 + 2\alpha_0) + \hat{n}(\beta_1 + \gamma_1 + 2\alpha_1) > 0$ , or  $(\beta_1 + \gamma_1)\alpha_0 < (\beta_0 + \gamma_0)\alpha_1$  and  $(1 - \hat{n})(\beta_0 + \gamma_0 + 2\alpha_0) + \hat{n}(\beta_1 + \gamma_1 + 2\alpha_1) < 0$ .

One can note from Fig. 1(C), that a Hopf bifurcation can arise in the olive and violet shaded regions, where, depending on the parameter values, the internal fixed point can lose its stability. In contrast, in the grey region, the fixed point remains a saddle point irrespective of the parameter values. Therefore, we focus on the olive and violet regions to determine the parameter criteria for the occurrence of a limit cycle.

1. *Olive region*: This region is demarcated by the inequality  $(\beta_1 + \gamma_1)\alpha_0 > (\beta_0 + \gamma_0)\alpha_1$ , hence the necessary and sufficient condition for  $\eta$  to be positive is  $(1 - \hat{n})(\beta_0 + \gamma_0 + 2\alpha_0) + \hat{n}(\beta_1 + \gamma_1 + 2\alpha_1) > 0$ . This condition is automatically satisfied because both  $(\beta_0 + \gamma_0 + 2\alpha_0)$  and  $(\beta_1 + \gamma_1 + 2\alpha_1)$  are positive throughout the olive region. Therefore, in either of the two cases, viz., (i)  $\beta_0 \geq \gamma_0$  and  $\beta_1 \leq \gamma_1$ , or (ii)  $\beta_0 \leq \gamma_0$  and  $\beta_1 \geq \gamma_1$ , a Hopf bifurcation occurs in the olive region, which corresponds to the 2nd and the 4th quadrants in Fig. 1(C)b.. Note that when the system moves directly from the third quadrant to the first quadrant in Fig. 1(C)b., by changing both parameters  $(\beta_0 - \gamma_0)$  and  $(\beta_1 - \gamma_1)$  from negative to positive simultaneously, a codimension-two Hopf bifurcation leads to the emergence of a limit cycle.

2. *Violet region*: This region is demarcated by the conditions  $\beta_1 + \gamma_1 > 0$  and  $\beta_0 + \gamma_0 + \alpha_0 < 0$ , which always satisfy the inequality  $(\beta_1 + \gamma_1)\alpha_0 > (\beta_0 + \gamma_0)\alpha_1$ .

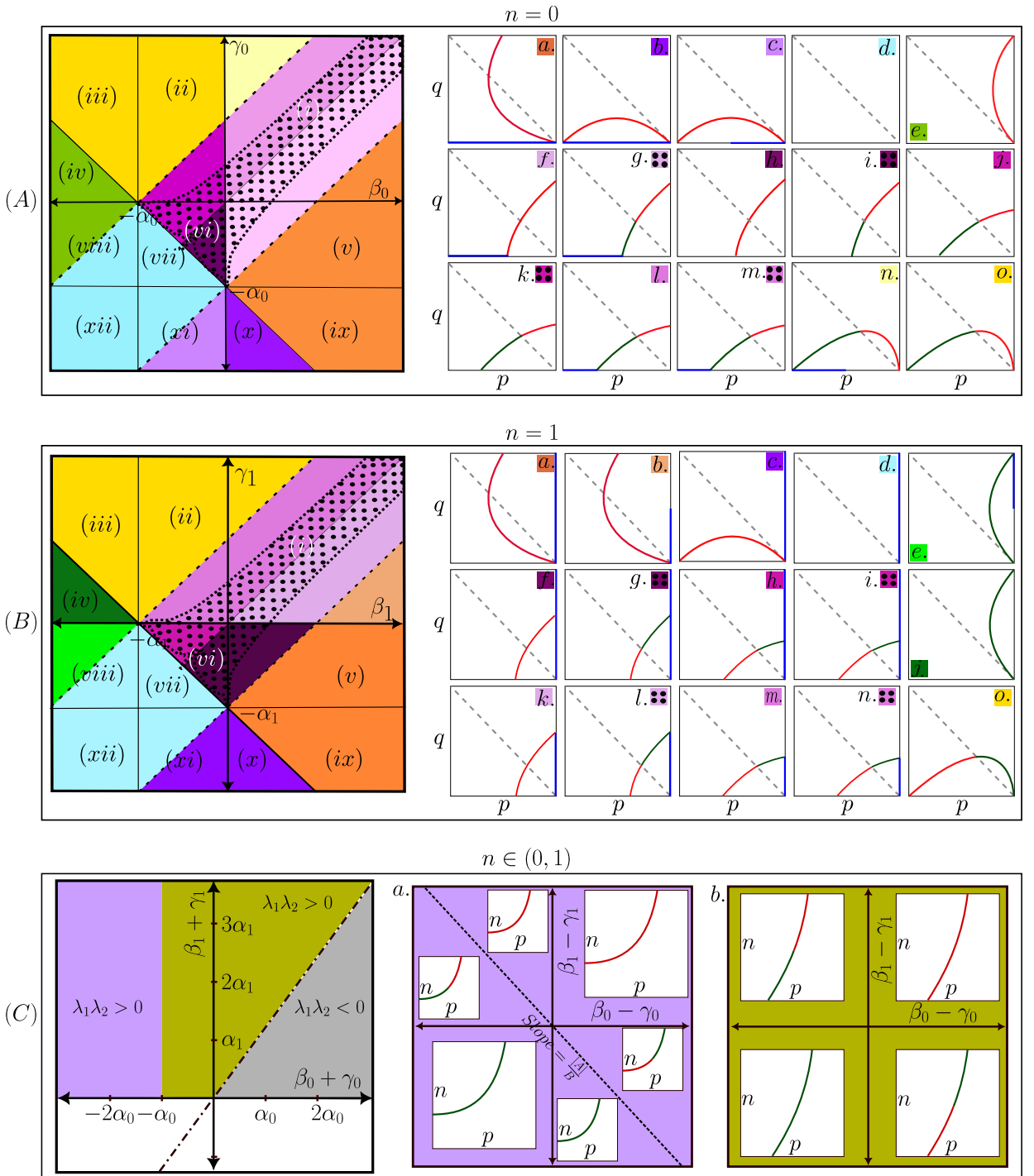


FIG. 1. An exhaustive depiction of parameter space detailing the stability of fixed-points. Panels (A) and (B) correspond to fixed-point lines arising from the intersections of the surfaces  $n = 0$  and  $F(p, q, n) = 0$ , and  $n = 1$  and  $F(p, q, n) = 0$ , respectively. The right-hand subpanels (a)–(o) illustrate the nature of stability of internal fixed-point structures corresponding to coloured parameter regions. Stable fixed-point curves appear in green, unstable fixed-point curves in red, and saturated fixed-point lines in blue. The dotted parameter region exhibits a distinctive feature, where the fixed-point line is partially stable and partially unstable. Panel (C) shows the stability behaviour of the internal fixed-point line corresponding to the intersection of the surfaces  $p + q = 1$  and  $F(p, q, n) = 0$ . Here  $\lambda_1\lambda_2$  is product of non-zero eigenvalues (see Eq. C1). The dot-dashed line corresponds to  $\beta_1 + \gamma_1 = \frac{\alpha_1}{\alpha_0}(\beta_0 + \gamma_0)$  and in subpanel a, the slope  $= \frac{|A|}{B} = -\frac{|\alpha_0 + \beta_0 + \gamma_0|}{\alpha_0 + \beta_1 + \gamma_1}$ . Twelve games different classes of distinct games, corresponding to different parameter regimes, are depicted in panels (A) and (B). They are labeled by (i) to (xii): Prisoner's dilemma (i), Chicken games (ii), Leader games (iii), Battle of sexes (iv), Stag-hunt (v), Harmony I (vi), Harmony II (vii), Deadlock II (viii), Coordination I (ix), Coordination II (x), Harmony III (xi), and Deadlock I (xii).

Hence, the necessary and sufficient condition for  $\eta$  to be positive, whenever  $\hat{n} \in [0, 1]$ , is  $(1 - \hat{n})(\beta_0 + \gamma_0 + 2\alpha_0) + \hat{n}(\beta_1 + \gamma_1 + 2\alpha_1) > 0$ , which is always true given the intermediate fixed points with  $q > 0$  exists (see Eq. (C3)). However, the admissible range of the equilibrium resource state is more constrained, because it attains its minimum physical value at  $n = n_m (> 0)$  (see Eq. (C7)). Since,  $n_m < \hat{n} \leq 1$ , this imposes stricter constraints on the parameter space: (i)  $\beta_0 \geq \gamma_0$  and  $\beta_1 \leq \gamma_1$ , and  $\alpha_1(\beta_0 - \gamma_0) + \alpha_0(\gamma_1 - \beta_1) > 2(\beta_1\gamma_0 - \gamma_1\beta_0)$ ; (ii)  $\beta_0 \leq \gamma_0$  and  $\beta_1 \geq \gamma_1$ , and  $\alpha_1(\beta_0 - \gamma_0) + \alpha_0(\gamma_1 - \beta_1) < 2(\beta_1\gamma_0 - \gamma_1\beta_0)$ . Cases (i) and (ii) correspond exactly to the region spanning the second and the fourth quadrants of Fig. 1(C)a, where some fixed points are stable while others are unstable. Note that when the system moves directly from the third quadrant to the first quadrant in Fig. 1(C)a—by changing both parameters  $(\beta_0 - \gamma_0)$  and  $(\beta_1 - \gamma_1)$  from negative to positive simultaneously—a codimension-two Hopf bifurcation can occur, leading to the emergence of a limit cycle.

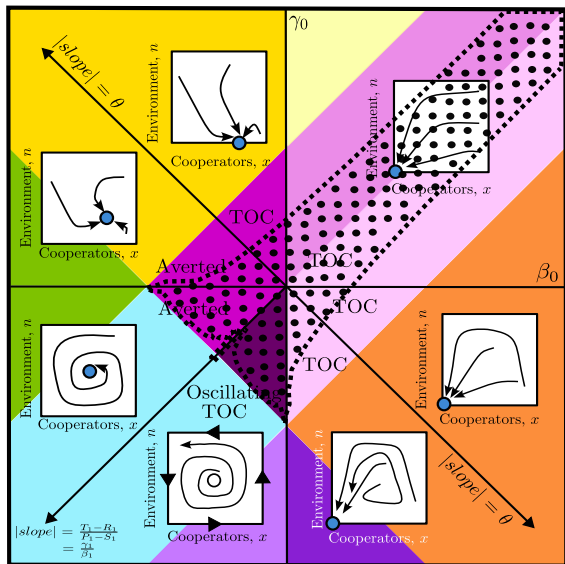


FIG. 2. A unified comparison of short- and long-term evolutionary dynamics across the  $\beta_0 - \gamma_0$  parameter space. The accompanying seven subplots (taken from ref. [51]) illustrate the short-term replicator dynamics mediated eco-evolutionary dynamics, with the  $x$ -axis representing the fraction of cooperators and the  $y$ -axis representing the fraction of the common resource. The  $x$ - $n$  phase-plane trajectories depict the stability of the isolated fixed point: open circles denote unstable fixed points, while filled colored circles represent stable ones. The parameter region in which the ToC is averted is labeled ‘Averted’. These should be compared with Figure 1 in its entirety; nevertheless, for the same of illustration we have put the backdrop of Figure 1(A) so that one can do comparison with the long-term adaptive dynamics with  $n = 0$  fixed point in focus.

### C. Comparison Between Long-Term and Short-Term Evolutionary Dynamics

From an evolutionary perspective, our analysis focuses on the long-term evolutionary process which is characterized by adaptive dynamics with additional feedback emanating from evolving resource state. We find it quite interesting that the reactive strategy space always contains some strategies around *tit-for-tat* (TFT) strategy ( $y = 1$ ,  $p = 1$ ,  $q = 0$ ) which can avert the ToC even for a defection-dominant strategy at both the replenished ( $n = 1$ ) and scarce ( $n = 0$ ) resource states. Moreover, the nonlinear feedback dynamics of strategy and resource can lead to a limit cycle kind of oscillation where the system ultimately settles down to an attractor where the strategy as well as resource state oscillates periodically due to the repeated invasion of the resident by mutants.

To motivate the significance of our results let us compare with the findings of a very recent paper ([51]) where they considered eco-evolutionary feedback dynamics involving one-shot game (instead of repeated interaction) and studied how the frequency ( $x$ ) of the cooperators and resource state co-evolve. The evolution of cooperator fraction followed replicator dynamics—a comparatively short-term dynamics. Fig. 2 captures the difference in evolutionary outcome between the short-term and the long-term dynamics. Short-term dynamics with one-shot game lead to three possible states: complete ToC ( $n = 0$ ), component ToC ( $0 < n < 1$ ), and oscillatory ToC (periodically changing  $n$ ); there is no possibility of complete aversion of ToC ( $n = 1$ ). In the long-term dynamics with repeated game, complete aversion of ToC is always possible for some initial choice of reactive strategy; however, for other strategies, the dynamics can lead to either complete, component ToC.

At first glance, this result may seem counterintuitive, since one might expect the outcomes in the short-term dynamics to be amplified in the long-term dynamics, given that the latter represents the cumulative effect of many short-term evolutionary steps. However, this contradiction is easily resolved once we consider the long-term eco-evolutionary feedback dynamics of (history-independent) reactive strategies, corresponding to  $p = q = x$  in our setting. In this case, the long-term dynamics exactly mirrors the evolutionary dynamics of the strategy frequency  $x$  in the model of Weitz *et al.* [51], which describes short-term evolution in a population with a fraction  $x$  of cooperators and  $1 - x$  of defectors under repeated mutant invasion. To see it explicitly, we have to substitute  $p = q = x$  and  $p' = q' = x'$  in Eq. (1), which gives  $C = x$  and  $C' = x'$ . Furthermore, the payoff Eq. (3) of the focal player after infinitely repeated interaction simplifies to

$$A = (\beta - \gamma)x'x - \beta x' + (\alpha + \gamma)x + P. \quad (12)$$

Therefore, the trait substitution sequence with eco-evolutionary feedback, incorporating resource dynamics given by Eq. (7) under both resource-evolution approaches,

leads to the following dynamical equations in the  $x$ - $n$  space:

$$\dot{x} = \frac{\partial S}{\partial x'} \Big|_{\{x'=x\}} = r(x)x(1-x)[r_1(x,n) - r_2(x,n)] \quad (13a)$$

$$\dot{n} = \varepsilon n(1-n)[\theta x - (1-x)], \quad (13b)$$

where,  $r(x) = 1/x(1-x)$ ,  $r_1(x,n) = [R_0(1-n) + R_1n]x + [S_0(1-n) + S_1n](1-x)$ , and  $r_2(x,n) = [T_0(1-n) + T_1n]x - [P_0(1-n) + P_1n](1-x)$ . Note that the form of the above equation is similar to the short-term eco-evolutionary feedback dynamics considered by Weitz et al. (see SI Appendix D in ref. [51]), except for a positive multiplicative factor  $r(x)$  appearing in front of Eq. (13a), which is finite since  $x = 0$  or 1 is not allowed in the reactive strategy space. One can easily verify that the stability of all fixed points is the same as in the short-term dynamics, except for the four boundary fixed points  $(0,0)$ ,  $(0,1)$ ,  $(1,0)$ , and  $(1,1)$ , which are not admissible in the reactive strategy space without boundaries as adopted in this paper. However, these boundary points act as saturation boundaries, and the conditions for reaching saturation points are exactly the same as the corresponding stability conditions in the short-term dynamics. Therefore, the qualitative conditions for ToC prevention remain unchanged relative to the short-term dynamics, with the only minor difference that oscillatory ToC [51] is replaced by stable limit-cycle oscillations. Main crux, however, is that allowing for the full reactive strategy space—which is infinitely larger than the binary choice of cooperating or defecting—introduces additional degrees of freedom that facilitate complete prevention of the ToC.

Although the proposed eco-evolutionary framework is sufficiently general to accommodate any symmetric  $2 \times 2$  game, it is too dense to render clearly understand the physical conditions under which ToC can be averted. To this end, the specific consideration of the Donation Game (DG) [97]—a canonical yet straightforward representation of social dilemmas in which defection is individually optimal but socially costly—can simplify the route of our understanding. Moreover, thanks to the general framework, the comparative role of reward and punishment in averting ToC, can be closely studied in the context of DG.

#### IV. AN APPLICATION: DONATION GAME WITH INSTITUTIONAL INCENTIVES

The DG—a simplified formulation of the PD game—offers one of the most transparent and analytically tractable frameworks for studying non-cooperative interaction systems observed in nature, where individuals face incentives to exploit shared resources or social partners [16, 98, 99]. Its explicit cost-benefit structure makes it particularly well-suited for investigating the conditions under which cooperation can avert the ToC. In this game, a player incurs a cost  $c$  whenever perform a cooperative act (and is then called a cooperator). In contrast, defectors obtain the benefit  $b$  ( $b > c > 0$ ) from interaction with cooperators without paying any cost. While mutual cooperation yields the socially optimal outcome, the

temptation to defect and obtain benefits without incurring costs drives the population toward behaviour that is individually advantageous yet collectively suboptimal. The payoff matrix of the DG is, thus, represented as follows:

		C (Cooperate)	D (Defect)	
		C (Cooperate)	$b - c, b - c$	$-c, b$
		D (Defect)	$b, -c$	0, 0

Following our general framework in Eq. (2), the environment-coupled payoff matrix becomes:

$$\Pi \equiv (1-n) \begin{bmatrix} b_0 - c & -c \\ b_0 & 0 \end{bmatrix} + n \begin{bmatrix} b_1 - c & -c \\ b_1 & 0 \end{bmatrix}, \quad (14)$$

where  $b_1$  and  $b_0$  (with  $b_1 > b_0 > c > 0$ ) are benefits at replete and deplete resource state, respectively.

#### A. Implementation of state dependent reward and punishment

In this simplest setting, our present interest is in investigating what comparative roles reward and punishment play in averting the ToC. To this end, we modify the payoff matrix so that a cooperative act against defection receive rewards and a defective act against cooperation incur punishment. Specifically, at deplete resource state ( $n = 0$ ), a cooperator (or donor) receives a reward  $\rho_0^+$  when interacting with a defector, whereas a defector incurs a punishment  $\rho_0^-$  for defecting against a cooperator. At the replete state ( $n = 1$ ), the corresponding modifiers are  $\rho_1^+$  and  $\rho_1^-$ , respectively. These extensions yield the following coupled payoff matrix:

$$\Pi = (1-n) \begin{bmatrix} b_0 - c & -c + \rho_0^+ \\ b_0 - \rho_0^- & 0 \end{bmatrix} + n \begin{bmatrix} b_1 - c & -c + \rho_1^+ \\ b_1 - \rho_1^- & 0 \end{bmatrix}. \quad (15)$$

Under such incentive structures, we expect that cooperation is more likely to be sustained; however, the interplay between reward and punishment is not clear *a priori*.

In terms of the parameters  $\alpha$ ,  $\beta$ , and  $\gamma$ , we have  $\gamma_0 = c - \rho_0^-$ ,  $\gamma_1 = c - \rho_1^-$ ,  $\beta_0 = c - \rho_0^+$ ,  $\beta_1 = c - \rho_1^+$ ,  $\alpha_0 = b_0 - c$  and  $\alpha_1 = b_1 - c$ . Since  $b_1 > b_0$ , it follows directly that  $\alpha_1 > \alpha_0$ . Thus, we now translate the general relations on  $\beta$ ,  $\gamma$ , and  $\alpha$  in terms of reward ( $\rho^+$ ), punishment ( $\rho^-$ ), benefit ( $b$ ), and cost ( $c$ ) to physically understand the conditions for ToC aversion and appearance of limit cycle in DG.

Firstly, following Fig. 1(A), one can directly talk about the conditions on reward ( $\rho_0^+$ ) and punishment ( $\rho_0^-$ ) for aversion complete ToC just by mapped from the parameter space  $\beta_0 - \gamma_0$  to the reward-punishment  $\rho^+ - \rho^-$  (see Fig. 3(a)). The axis  $\beta_0 = 0$  and  $\gamma_0 = 0$  corresponds to  $\rho_0^+ = c$  and  $\rho_0^- = c$ , and conditions  $\beta_0 + \gamma_0 = -\alpha_0$  and  $\beta_0 - \gamma_0 = \alpha_0$  correspond to  $\rho_0^+ + \rho_0^- = b_0 + c$  and  $\rho_0^+ - \rho_0^- = c - b_0$ , respectively.

Similarly, following Fig. 1(C), the region corresponding to partial or component ToC at the intermediate resource state  $n \in (0, 1)$  is mapped from the parameter space  $\beta_0 - \gamma_0$  to reward-punishment  $\rho_0^+ - \rho_0^-$ , under the conditions  $\rho_1^+ > \rho_1^-$

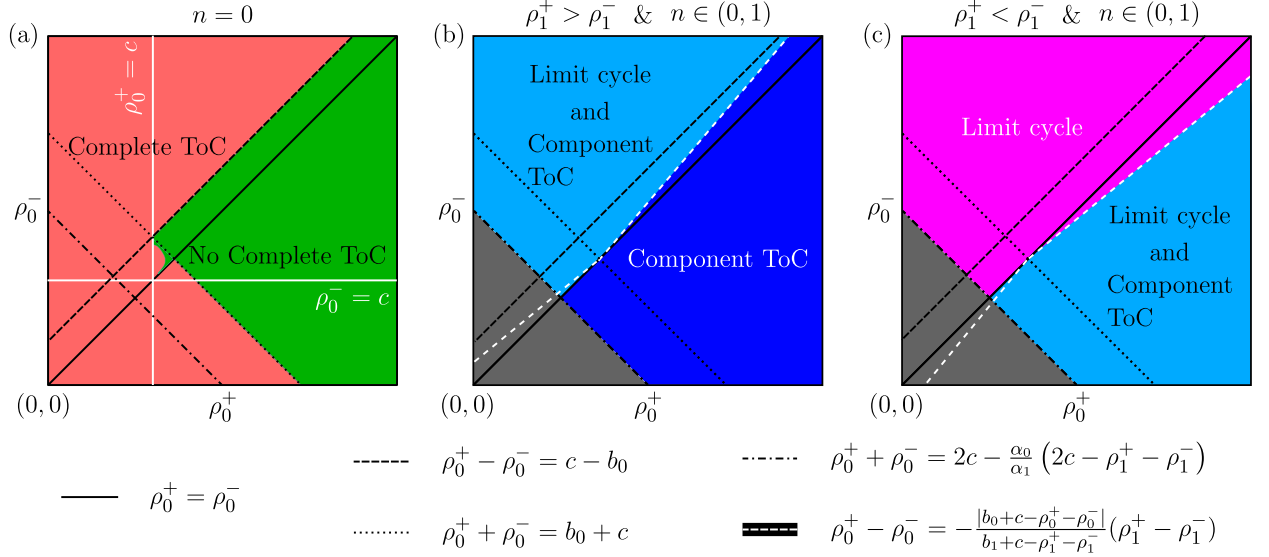


FIG. 3. ToC and its prevention in the reward ( $\rho_0^+$ )–punishment ( $\rho_0^-$ ) parameter space. Subplot (a) shows the stability properties of the fixed points on the  $n = 0$  plane. The green region corresponds to parameter values for which the fixed points are either completely unstable or do not exist; consequently, for any initial choice of reactive strategy, complete ToC is avoided in this region. In contrast, this is not possible in the light-red shaded region, where a stable fixed point exists on the  $n = 0$  plane. Subplots (b) and (c) show the stability properties of internal fixed points over the admissible range of reward and punishment. The light-blue region represents internal fixed points that are partially stable and partially unstable, while the dark-blue region corresponds to completely stable internal fixed points. The gray and magenta regions denote saddle and completely unstable internal fixed points, respectively. The corresponding dynamical outcomes in these regions are also indicated.

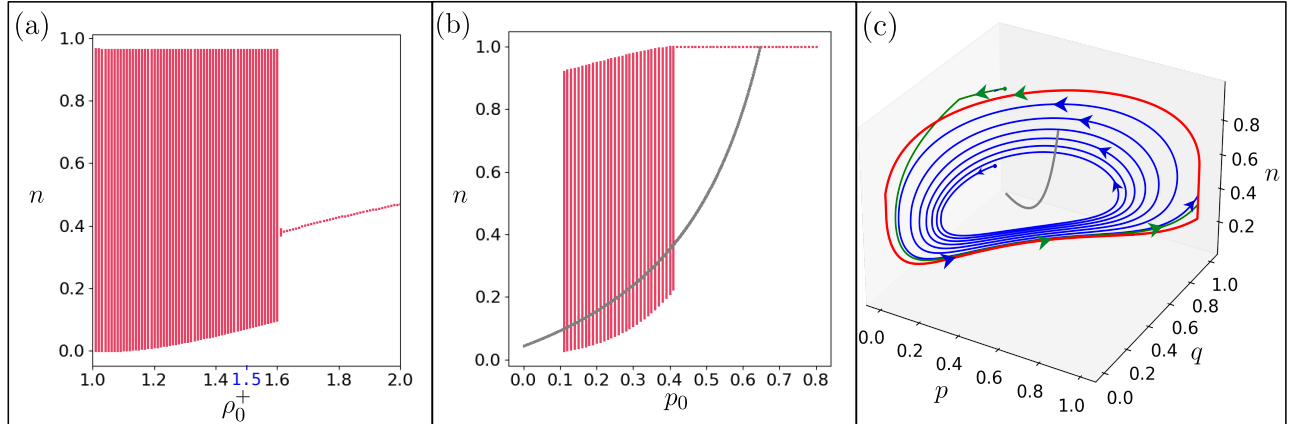


FIG. 4. Limit cycles through a Hopf bifurcation in the presence of reward and punishment. Subplot (a) shows the Hopf bifurcation scenario resulting from variation of the parameter  $\rho_0^+$  while keeping  $\rho_0^- = 1.6$  fixed. For  $\rho_0^+ > \rho_0^-$ , the system stabilizes at a fixed point, indicating steady-state behaviour. As  $\rho_0^+$  crosses the critical threshold  $\rho_0^+ = \rho_0^-$ , a Hopf bifurcation occurs, leading to the emergence of sustained oscillations in  $n$  for  $\rho_0^+ < \rho_0^-$ . Subplots (b) and (c) correspond to the specific parameter value  $\rho_0^+ = 1.5$ . Subplot (b) illustrates the occurrence of a continuum of limit cycles in the  $n-p_0$  space, where  $n$  denotes the evolving resource state and  $p_0$  represents the initial reciprocity, while the initial generosity is fixed at  $q_0 = 0.4$ . The gray solid curve represents a continuous set of unstable fixed points. Subplot (c) visualizes the limit cycles for two different initial conditions,  $(p = 0.14, q = 0.66, n = 0.46)$  and  $(p = 0.12, q = 0.77, n = 0.85)$ . The trajectories, shown by green and blue solid curves, converge to a closed orbit (red curve) surrounding the gray solid unstable fixed-point curve. The remaining parameters used in these plots are  $\rho_0^- = 1.6$ ,  $\rho_1^+ = \rho_1^- = 0.5$ ,  $b_1 = 2.2$ ,  $b_0 = 2.0$ , and  $c = 1$ .

and  $\rho_1^+ < \rho_1^-$  (see Fig. 3(b) and Fig. 3(c)). The detailed calculations are shown in Appendix D.

Finally, the conditions for Hopf bifurcation in reward-punishment parameter space, which is archived just by transforming the conditions of Hopf bifurcation calculated in terms of  $\beta$ ,  $\gamma$  in Section III B in terms of  $\rho^+$ ,  $\rho^-$  as follows: The condition  $\rho_0^+(b_1 + c - 2\rho_1^-) - \rho_0^-(b_1 + c - 2\rho_1^+) = (\rho_1^+ - \rho_1^-)(b_0 + c)$  corresponds to  $\alpha_1(\beta_0 - \gamma_0) + \alpha_0(\gamma_1 - \beta_1) = 2(\beta_1\gamma_0 - \gamma_1\beta_0)$  and  $\rho_0^+ + \rho_0^- = \frac{(\alpha_1 - \alpha_0)2c}{\alpha_1} + \frac{\alpha_0}{\alpha_1}(\rho_1^+ + \rho_1^-)$  correspond to constraint  $(\beta_1 + \gamma_1)\alpha_0 = (\beta_0 + \gamma_0)\alpha_1$ .

## B. Results

- (i) It is evident from Fig. 1(B) that, for any choice of parameter values, either stable fixed points or saturation points exist. Thus, for any values of reward and punishment, there always exists a reactive strategy close to TFT such that choosing it allows one to avert the ToC and attain the maximum resource state.
- (ii) The necessary condition to avert complete ToC for all possible initial choices of reactive strategies is  $\rho_0^+ > c$  (see Fig. 3(a)).
- (iii) Fig. 3(a) shows that sufficiently high reward in the depleted resource state leads to the aversion of the complete ToC irrespective of the amount of punishment. In contrast, when punishment exceeds reward, the effectiveness of averting complete ToC depends on how much the benefit  $b_0$  is more than the cost  $c$ —larger differences resulting in higher possibility of ToC mitigation by rewarding and punishing.
- (iv) One more fact can be read from Fig. 3(a): Complete ToC is precluded for all initial reactive strategies when the reward-punishment parameters at the depleted resource state satisfy  $\rho_0^+ + \rho_0^- > c + b_0$  and  $\rho_0^+ - \rho_0^- > c - b_0$ . These conditions can be recast as  $\rho_0^+ - c > b_0 - \rho_0^-$  and  $(\rho_0^+ - c) + (b_0 - \rho_0^-) > 0$ , respectively. In game-theoretic terms, this corresponds to a Harmony-type interaction in the depleted state, where cooperation is a strictly dominant strategy. In particular, when one player cooperates while the opponent defects, the cooperator receives a higher payoff than the defector, and the sum of the two players' payoffs exceeds that obtained when both defect.
- Moreover, even when the condition  $\rho_0^+ - c > b_0 - \rho_0^-$  is violated, there exist region with punishment exceeding reward for which complete ToC can still be averted for all initial strategy choices. This region increases with the difference  $(b_0 - c)$  between benefit and cost in the deplete resource state.
- (v) As per Fig. 3(b)-(c), below the dot-dashed (gray region), i.e., when  $\frac{\alpha_0}{\alpha_1}(2c - \rho_1^+ - \rho_1^-) < 2c - \rho_0^+ - \rho_0^-$ , intermediate resource states—either through limit cycles or component ToC—are impossible. In this region, the dynamical outcome is bistable: depending on

the initial strategy choice, the system evolves either to complete ToC or to aversion of ToC. Consequently, the long-term outcome becomes highly sensitive to the initial strategy choice, and some initial strategies may lead to severe resource depletion. This region corresponds to a defection-dominant payoff structure in the depleted state, given that defection is already the dominant strategy in the replete state. Moreover, the extent of this region depends on the ratio  $(\alpha_0/\alpha_1)$  of the benefit-cost differences between the depleted and replete states. When the benefit-cost difference in the depleted state is smaller than that in the replete state, this region is more likely to occur. Interestingly, when the magnitudes of benefit and cost are equal in the replete state, this region is never reached, and intermediate resource levels are always observed, even under defection-dominated payoffs.

- (vi) In the region above the dotted line, bounded by the white dashed line and the black dashed line, in Fig. 3(c), the dynamics either lead to limit-cycle oscillations or to the maximum resource state [note also Fig. 3(a)]. Interestingly, our numerical results show that when the punishment in the replete state is equal to the cost, and for any allowed value of the reward, the long-term eco-evolutionary feedback dynamics always converge to the maximum resource state for all possible initial choices of reactive strategies.
- (vii) Our numerical analysis illustrates the occurrence of a Hopf bifurcation for fixed parameter values  $\rho_0^- = 1.6$  and  $\rho_1^+ = \rho_1^- = 0.5$  (see Fig. 4(a)). In this regime, the reward-punishment mechanism can give rise to periodically oscillatory evolutionary outcomes, such as stable limit cycles, in which both the reactive strategies and the resource state oscillate indefinitely. Moreover, a continuum of limit cycles can exist (Fig. 4(b)), and different limit cycles are selected depending on the initial choice of strategy. An important consequence is that, for certain initial conditions, the corresponding limit-cycle orbit may approach near-total resource depletion. However, such outcomes can be avoided by choosing alternative initial conditions that lead to limit cycles along which the resource level remains high enough.

## V. CONCLUSIONS

A key result of our comprehensive analysis is the qualitative contrast between short-term and long-term evolutionary outcomes in  $2 \times 2$  games in shaping the ToC. Short-term dynamics—driven by one-shot interaction and population-level frequency updates—exhibit either complete ToC or component ToC; complete aversion of ToC is impossible in this regime. In contrast, long-term mutation-selection dynamics—driven by repeated interactions and trait substitution sequences in the reactive strategy space—can give rise to complete aversion of ToC for all parameter values when the population adopts reactive strategies close to TFT.

The introduction of reward and punishment mechanisms fundamentally reshapes the effective payoff landscape experienced by individuals, thereby influencing their cooperative or defective tendencies. Through modifying the relative costs and benefits associated with resource use, these mechanisms stabilize cooperative behaviour and suppress exploitative strategies that would otherwise drive the system toward the ToC. Importantly, this influence persists even over long evolutionary timescales, where transient advantages are filtered out and only dynamically stable outcomes remain. Thus, reward and punishment do not merely produce short-term compliance but instead contribute to the emergence of sustained, system-level regulation of shared resources.

A significant amount of work has been conducted on the basis of rewards and punishments to explore the emergence of cooperation, which is directly intertwined with ToC. Let us summarize how direct rewards and punishment, either alone or combined, have an impact on the Aversion of ToC. The punishment leads more effectively has a significant importance to avert ToC in the work [55, 82–84, 100]; specifically, Kerava [100] studied both adaptive dynamics and replicator dynamics averting ToC for a one-shot game with reward and punishment, and has concluded that the punishment has more importance than rewards in those scenarios.

Our results further demonstrate that rewards and punishments applied in the depleted resource state have a subtle impact on averting ToC. This effect is constrained by the cost–benefit parameters and is particularly evident in regimes dominated by punishment. In contrast, in the intermediate resource regime—where punishment at the replete state exceeds reward—the depleted-state punishment exerts a robust influence on partial ToC aversion through the emergence of limit cycles, whereas depleted-state rewards tend to promote component ToC accompanied by limit-cycle dynamics. We also observe that even when reward dominate punishment at high values, averting ToC can still occur, either via component ToC or through limit-cycle behaviour. The periodically oscillatory evolutionary outcomes, via a limit cycle, where both reactive strategies and resource state oscillate indefinitely is indeed an interesting feature of our model. All these findings imply that institutional rewards alone may be insufficient to sustain cooperation in resource-sharing systems.

Before we conclude, we would like to highlight that in the paradigm of adaptive dynamics, a central question concerns the fate of trait evolution—whether the population remains monomorphic or undergoes evolutionary branching [67]. Understanding how evolutionary branching is affected by the co-evolving environmental resources constitutes an important open direction for exploration.

## ACKNOWLEDGMENTS

Abhishek Yogi is thanked for his inputs during the initial stages of this work. Financial assistance from the University Grants Commission (UGC), New Delhi, in the form of a Senior Research Fellowship is gratefully acknowledged by the first author.

## Appendix A: Non-isolated fixed points at the intersection of surfaces— $n = 0$ and $F(p, q, n) = 0$

The eigenvalues of the Jacobian matrix at the deplete state ( $n = 0$ ) are given by:

- (i)  $\lambda_1 = (p + q - 1)$ ,
- (ii)  $\lambda_2 = q[q(\beta_0 - \gamma_0) + (1 - 2r)(\alpha_0 + \gamma_0) + \beta_0] + (1 - p)[(1 + r)(\beta_0 - \gamma_0) - q(\beta_0 - \gamma_0) - (1 - 2r)(\alpha_0 + \gamma_0) - \beta_0]$ ,
- (iii)  $\lambda_3 = 0$ .

The zero eigenvalue  $\lambda_3 = 0$  indicates neutral stability along the corresponding eigenvector, meaning that small perturbations in this direction does not time-evolve. Naturally, the fixed points and their stability at  $n = 0$  depend solely on the game played at the depleted state and are independent of the game played at  $n = 1$ . The existence and stability properties of the non-isolated fixed points and boundary points at the depleted state are analyzed in detail below with a view to showing how Subplot (A) of Fig. (1) is constructed to exhibit the distinct stability regions associated with different underlying games.

### 1. Construction of Fig. 1(A)

To fully determine the stability of the continuous line of fixed points, we must know the signs of both eigenvalues  $\lambda_1$  and  $\lambda_2$ . The sign of  $\lambda_1$  can be readily inferred from the structure of the fixed points:  $\lambda_1 > 0$  for fixed points lying above the line  $p + q = 1$ —shown in gray dashed line in subplots, and  $\lambda_1 < 0$  for those below it. In contrast, predicting the sign of  $\lambda_2$  along the continuous line of fixed points is more challenging because of its complex functional dependence. However, we identify a simpler approach that allows us to determine the sign of  $\lambda_2$  for all fixed points and parameter combinations.

#### a. Predicting the Sign of $\lambda_2$

The eigenvector corresponding to  $\lambda_2$  is orthogonal to the resource direction and lies entirely within the  $p$ – $q$  plane. Hence, the sign of  $\lambda_2$  is determined exclusively by the dynamics of the reactive strategies Eq. (5a) and Eq. (5b) in the vicinity of  $n = 0$ .

In the resulting two-dimensional setting at  $n = 0$ , the behavior is straightforward: if  $F(p, q, 0) > 0$ , then  $\dot{p} > 0$  and  $\dot{q} > 0$ ; if  $F(p, q, 0) < 0$ , then  $\dot{p} < 0$  and  $\dot{q} < 0$ . A continuous line of fixed points arises precisely when  $F(p, q, 0) = 0$ . Thus, by determining the sign of  $F(p, q, 0)$  above and below this line, we can directly infer the stability of the fixed points—or equivalently, the sign of  $\lambda_2$ .

First, we rewrite the function  $F(p, q, 0)$  in a more convenient form:

$$F(p, q, 0) = f(c, r) \equiv \frac{(\beta_0 - \gamma_0)}{2}c(1 + r) - \frac{(\beta_0 - \gamma_0)}{2}r(1 + r) + (\alpha_0 + \gamma_0)r(1 - r) - \beta_0(1 - r), \quad (\text{A1a})$$

where  $c = p + q$ . Note that the curves  $c = a_1$  and  $r = p - q = a_2$  (with  $a_1$  and  $a_2$  being arbitrary constants) are orthogonal in the  $p$ - $q$  coordinate plane; i.e.,  $c$  and  $r$  form two independent coordinates. Thus, we can vary the value of  $c$  while keeping  $r$  fixed.

Consider an arbitrary point with  $c = c^*$  and  $r = r^*$  on the continuous line of fixed points. If we increase the value of  $c$  from  $c^*$  while keeping  $r$  unchanged, and if  $\beta_0 > \gamma_0$ , then  $f(c, r) > 0$ , which implies  $\dot{p} > 0$  and  $\dot{q} > 0$  (see Eq. 5). Conversely, if we decrease the value of  $c$  from  $c^*$ , then for  $\beta_0 > \gamma_0$  we obtain  $f(c, r) < 0$ , yielding  $\dot{p} < 0$  and  $\dot{q} < 0$ . A similar argument holds for  $\beta_0 < \gamma_0$ , if  $c$  is increased (decreased) from  $c^*$ , then  $f(c, r) < 0$  ( $f(c, r) > 0$ ), implying  $\dot{p} < 0$ ,  $\dot{q} < 0$  ( $\dot{p} > 0$ ,  $\dot{q} > 0$ ). Therefore, for  $\beta_0 > \gamma_0$ , the eigenvalue  $\lambda_2$  at the fixed point corresponding to  $(c^*, r^*)$  is positive, while for  $\beta_0 < \gamma_0$ , it is negative. Since the argument holds for any arbitrary fixed point on the continuous line, the conclusion applies to the entire line of fixed points.

Caution needs to be exercised in the magenta region shown in Fig. 5(a), where the sign of  $\lambda_2$  may differ at different points along the same fixed-point line due to its special structure. As shown in Fig. 5(b), even though increasing (decreasing)  $c$  from  $c^*$  at fixed  $r$  always leads to  $f(c, r) < 0$  ( $f(c, r) > 0$ ) for fixed values of  $\beta_0$  and  $\gamma_0$ , certain segments of the fixed-point line are stable while others are unstable. The underlying reason is that the orbits of the evolutionary dynamics in the  $p$ - $q$  space intersect the fixed-point line twice. Consequently, although our method—based on the sign of  $f(c, r)$  in Eq. (A1) evaluated at  $n = 0$ —correctly predicts the direction of flow throughout the phase space, the sign of  $\lambda_2$  may still vary depending on the precise location along the fixed-point line. This behavior is exhibited by the fixed-point line corresponding to the dotted region of parameter space in Subplots (A) and (B) of Fig. 1.

### b. Predicting the sign of $\lambda_1$

Determining the sign of  $\lambda_1$  requires knowledge of the structure of the fixed-point line for different parameter values. Specifically, if the fixed-point line (or a segment of it) lies above the line  $p + q = 1$ , then  $\lambda_1 < 0$  along that segment. Conversely, if the fixed-point line (or a segment of it) lies below the line  $p + q = 1$ , then  $\lambda_1 > 0$ .

The function  $F(p, q, 0)$  is always zero at  $p = 1$  and  $q = 0$ ; i.e., the continuous line of fixed points always passes through point  $(1, 0)$ . By examining the slope of this fixed-point line at  $(1, 0)$  point and determining the parameter conditions under which the fixed-point curve intersects the line  $p + q = 1$ , we can divide the parameter space into six different regions, each exhibiting a different fixed-point structure. These six regions are shown in Subplot (A) of Fig. (1), represented by six different colours, viz., orange, cyan, green, yellow, violet, and magenta (different shades of same colours are also used).

### c. Demarcation of six regions in the parameter space

At the  $n = 0$  plane, the continuous line of fixed points satisfies  $F(p, q, 0) = 0$ , which in explicit form can be written as

$$-(\alpha_0 + \gamma_0)p^2 - (\alpha_0 + \beta_0)q^2 + (2\alpha_0 + \beta_0 + \gamma_0)pq + (\alpha_0 + \beta_0 + \gamma_0)p - (\alpha_0 + 2\gamma_0)q - \beta_0 = 0. \quad (\text{A2})$$

This equation defines a hyperbola, and it is straightforward to verify that the point  $(1, 0)$  is always a solution for all admissible parameter values. The slope of the curve at the point  $(1, 0)$  relative to the  $q = 0$  axis is given by

$$\frac{dq}{dp} = -\frac{(\beta_0 - \gamma_0) - \alpha_0}{(\beta_0 - \gamma_0) + \alpha_0}. \quad (\text{A3})$$

To determine whether the continuous line of fixed points intersects the line  $p + q = 1$  at a point other than  $(1, 0)$ , we substitute  $p = 1 - q$  into Eq. (A2). This yields a quadratic equation in  $q$ , whose solutions are  $q = 0$  and  $q = \alpha_0/(2\alpha_0 + \beta_0 + \gamma_0)$ . The solution  $q = \alpha_0/(2\alpha_0 + \beta_0 + \gamma_0)$  provides us with new information, where the intersection point of the continuous line of fixed points and the  $p + q = 1$  line is physical when  $\alpha_0/(2\alpha_0 + \beta_0 + \gamma_0) \in (0, 1]$ , which implies:

$$\frac{\alpha_0}{2\alpha_0 + \beta_0 + \gamma_0} > 0 \implies (\beta_0 + \gamma_0) > -2\alpha_0, \quad (\text{A4a})$$

$$\frac{\alpha_0}{2\alpha_0 + \beta_0 + \gamma_0} \leq 1 \implies (\beta_0 + \gamma_0) \geq -\alpha_0. \quad (\text{A4b})$$

It is evident that the condition in Eq. (A4b) is stronger and therefore automatically implies condition (A4a). Hence, we conclude that the continuous line of fixed points intersects the line  $p + q = 1$  at a second physical point (in addition to  $(1, 0)$ ) whenever  $(\beta_0 + \gamma_0) \geq -\alpha_0$ .

We next characterize the possible configurations of the continuous line of fixed points. There are two cases in which the tangent angle of this curve at  $(1, 0)$ , measured relative to the  $q = 0$  axis, lies in the interval  $[\pi/2, \pi]$ .

1.  $|(\beta_0 - \gamma_0) - \alpha_0| > |(\beta_0 - \gamma_0) + \alpha_0|$

This case occurs only when  $(\beta_0 - \gamma_0) \leq -\alpha_0$ .

- When  $(\beta_0 - \gamma_0) \leq -\alpha_0$  and  $(\beta_0 + \gamma_0) \geq -\alpha_0$ , the continuous line of fixed points has a tangent angle  $\phi$  at  $(1, 0)$  that is in the range  $3\pi/4 < \phi < \pi/2$  and intersects the line  $p + q = 1$  within the physical region. Therefore, in this parameter region,  $\lambda_1 < 0$  on some segments of the fixed-point line and  $\lambda_1 > 0$  on others, as indicated by the yellow region in Fig. 1(A).
- When  $(\beta_0 - \gamma_0) \leq -\alpha_0$  but  $(\beta_0 + \gamma_0) < -\alpha_0$ , the continuous line of fixed points again has a tangent angle  $\phi$  at  $(1, 0)$  that is in the range  $3\pi/4 < \phi < \pi/2$  but does not intersect the line  $p + q = 1$ . Therefore, in this parameter region,  $\lambda_1 > 0$  everywhere, and the fixed-point line is completely unstable, as indicated by the green region in Fig. 1(A).

2.  $|\beta_0 - \gamma_0| < |\beta_0 - \gamma_0| + \alpha_0|$

This case occurs only when  $(\beta_0 - \gamma_0) \geq \alpha_0$ .

- (i) When  $(\beta_0 - \gamma_0) \geq \alpha_0$  and  $(\beta_0 + \gamma_0) \geq -\alpha_0$ , the continuous line of fixed points has a tangent angle  $\phi$  at  $(1, 0)$  that is in the range  $\pi < \phi < 3\pi/4$  and intersects the line  $p + q = 1$  within the physical region. Therefore, in this parameter region,  $\lambda_1 < 0$  on some segments of the fixed-point line and  $\lambda_1 > 0$  on others. This corresponds to the orange region in Fig. 1(A). Nevertheless, the fixed-point line is completely unstable in this parameter range because  $\lambda_2 > 0$  everywhere.
- (ii) When  $(\beta_0 - \gamma_0) \geq \alpha_0$  but  $(\beta_0 + \gamma_0) < -\alpha_0$ , the continuous line of fixed points has a tangent angle

$\phi$  at  $(1, 0)$  that is in the range  $\pi < \phi < 3\pi/4$  but does not intersect the line  $p + q = 1$ . Therefore, in this parameter region,  $\lambda_1 < 0$  everywhere. This corresponds to the violet region in Fig. 1. However, the fixed-point line is completely unstable in this parameter range because  $\lambda_2 > 0$  throughout the region.

When  $-\alpha_0 < (\beta_0 - \gamma_0) < \alpha_0$ , the branch of the hyperbola passing through the point  $(1, 0)$  lies outside the physical region. However, other portions of the same hyperbola remain within the physical region. In such cases, the fixed-point curve must intersect the boundary of the physical region at points other than  $(1, 0)$ . The possible boundaries and the corresponding crossing points are given below:

$$(i) p = 1 \implies q = 1 - \frac{\gamma_0}{\alpha_0 + \beta_0}, \quad (A5a)$$

$$(ii) p = 0 \implies q_{\pm} = \frac{1}{2(\alpha_0 + \beta_0)} \left[ -(\alpha_0 + 2\gamma_0) \pm \sqrt{(\alpha_0 + 2\gamma_0)^2 - 4\beta_0(\alpha_0 + \beta_0)} \right], \quad (A5b)$$

$$(iii) q = 0 \implies p = \frac{\beta_0}{(\alpha_0 + \gamma_0)}, \quad (A5c)$$

$$(iv) q = 1 \implies p_{\pm} = \frac{1}{2(\alpha_0 + \gamma_0)} \left[ (3 + 2\beta_0 + 2\gamma_0) \pm \sqrt{(3\alpha_0 + 2\beta_0 + 2\gamma_0)^2 - 8(\alpha_0 + \gamma_0)(\alpha_0 + \beta_0 + \gamma_0)} \right]. \quad (A5d)$$

Within the parameter region  $-\alpha_0 < (\beta_0 - \gamma_0) < \alpha_0$  and  $(\beta_0 + \gamma_0) \geq -\alpha_0$ , the fixed-point curve defined by Eq. (A2) always intersects the line  $p + q = 1$  at a point other than  $(1, 0)$ , and this lies within the physical region. Consequently, a branch of the fixed-point curve that does not pass through  $(1, 0)$  always exists whenever  $(\beta_0 + \gamma_0) \geq -\alpha_0$ . Moreover, since the fixed-point line crosses the line  $p + q = 1$ ,  $\lambda_1 > 0$  on some portions of it and  $\lambda_1 < 0$  on the remaining portions. This parameter regime corresponds to the pink region in Fig. 1(A).

We next consider the case  $(\beta_0 + \gamma_0) < -\alpha_0$  together with  $-\alpha_0 < (\beta_0 - \gamma_0) < \alpha_0$ . In this region, both  $\beta_0$  and  $\gamma_0$  are negative as indicated by Fig. 1(A). Since no branch of the fixed-point curve intersects the line  $p + q = 1$  in this regime, the only remaining question is whether more than one boundary fixed point—corresponding to the cases listed in (i.e., (A5a), (A5b), (A5c), (A5d)) can exist.

- (i) Since in our region of interest,  $(\alpha_0 + \beta_0) > \gamma_0$  always holds, and  $\beta_0$  and  $\gamma_0$  are always negative, we can directly conclude that the fixed point at  $p = 1$  and  $q = 1 - \gamma_0/(\alpha_0 + \beta_0)$  is not physical.
- (ii) (a) When  $(\alpha_0 + \beta_0) < 0$ , the necessary condition for the fixed point (A5b) (both  $q_+$  and  $q_-$ ) to be physical is  $(\alpha_0 + 2\gamma_0) > 0$  and  $|2(\alpha_0 + \beta_0)| > |(\alpha_0 + 2\gamma_0)|$ . However, in that case, the term inside the square root is negative, and the fixed points become imaginary.

- (b) When  $(\alpha_0 + \beta_0) > 0$ , then the necessary condition for the fixed point to exist is  $(\alpha_0 + 2\gamma_0) < 0$ . For both the fixed points, corresponding to  $q_+$  and  $q_-$ , to be greater than or equal to zero, the necessary condition is the following:

$$-(\alpha_0 + 2\gamma_0) > \sqrt{(\alpha_0 + 2\gamma_0)^2 - 4\beta_0(\alpha_0 + \beta_0)}.$$

The above equation ultimately boils down to  $0 > -4\beta_0(\alpha_0 + \beta_0)$ , which is impossible as  $\beta_0 < 0$  in our case.

- (iii) In light of the domain of interest,  $\beta_0 < (\alpha_0 + \gamma_0)$  always, and  $\beta_0$  and  $\gamma_0$  are always negative, we can directly conclude that the fixed point at  $p = \beta_0/(\alpha_0 + \gamma_0)$  and  $q = 0$  can't be physical.
- (iv) (a) When  $(\alpha_0 + \gamma_0) > 0$ , the following condition need to satisfy for  $p_{\pm} \geq 0$ :

$$\frac{(3\alpha_0 + 2\beta_0 + 2\gamma_0)}{\pm \sqrt{(3\alpha_0 + 2\beta_0 + 2\gamma_0)^2 - 8(\alpha_0 + \gamma_0)(\alpha_0 + \beta_0 + \gamma_0)}} \geq 0.$$

It ultimately implies,  $-8(\alpha_0 + \gamma_0)(\alpha_0 + \beta_0 + \gamma_0) \leq 0$ , which is impossible because  $(\alpha_0 + \beta_0 + \gamma_0) < 0$  for our case. So we can conclude that for  $(\alpha_0 + \gamma_0) > 0$ ,  $p_{\pm}$  can not be non-negative.

- (b) When  $(\alpha_0 + \gamma_0) < 0$ , sign of  $(\alpha_0 + \gamma_0)$  have to be same with the sign of  $(3\alpha_0 + 2\beta_0 + 2\gamma_0)$ , otherwise, one of the fixed point is negative. Now, if

$2|\alpha_0 + \gamma_0| \geq |3\alpha_0 + 2\beta_0 + 2\gamma_0|$ , then  $2|\alpha_0 + \gamma_0 + \beta_0| > |3\alpha_0 + 2\beta_0 + 2\gamma_0|$ ; since  $\beta_0$  and  $\gamma_0$  are always negative, therefore,  $|\alpha_0 + \gamma_0 + \beta_0| > |\alpha_0 + \gamma_0|$ . So the term inside the square root becomes negative, and the fixed points become imaginary. If, on the other hand,  $2|\alpha_0 + \gamma_0| < |3\alpha_0 + 2\beta_0 + 2\gamma_0|$  then the first term becomes greater than one and one of the fixed points should surely be outside the physical region.

So, we can conclude that in the region such that  $-\alpha_0 < (\beta_0 - \gamma_0) < \alpha_0$  and  $(\beta_0 + \gamma_0) < -\alpha_0$ , i.e., in the cyan region of Fig. (1), no fixed point line can exist inside the physical region.

We next examine the boundary points and determine whether they are saturated in each parameter region. At  $n = 0$ , the saturated boundary points can occur only along the boundary  $q = 0$  (as discussed in Section III). A boundary point on  $q = 0$  is saturated only when it satisfies the following relation:

$$(\alpha_0 + \gamma_0)p < \beta_0, \quad \forall p \in [0, 1]. \quad (\text{A6})$$

*Orange zone:* Since in this region  $\beta_0 > \alpha_0 + \gamma_0$  and  $\beta_0 > 0$ , the boundary  $q = 0$  consists entirely of saturated points for all  $p \in [0, 1]$ .

*Violet zone:* In this region  $\beta_0 > \alpha_0 + \gamma_0$  and  $(\alpha_0 + \gamma_0) < 0$ . The behaviour of boundary points depends on the sign of  $\beta_0$ . When  $\beta_0 > 0$ , all the boundary points are saturated (Subplot b.). In contrast, when  $\beta_0 < 0$ , only those boundary points near  $(1, 0)$  are saturated (Subplot c.), in accordance with Eq. (A6).

*Yellow zone:* In this region  $\beta_0 < \alpha_0 + \gamma_0$  and  $\alpha_0 + \gamma_0 > 0$ . Again, the behaviour of boundary points depends on the sign of  $\beta_0$ . When  $\beta_0 > 0$ , some of the boundary points are saturated (Subplot g.). In contrast, when  $\beta_0 < 0$ , no boundary point is saturated (Subplot f.), in accordance with Eq. (A6).

*Green zone:* In this region  $\beta_0 < \alpha_0 + \gamma_0$  and  $\beta_0 < 0$ , the boundary  $q = 0$  has no saturated point.

*Magenta zone:* Although the condition  $\beta_0 < (\alpha_0 + \gamma_0)$  holds throughout this region, the behaviour of the boundary points depends on the sign of  $\beta_0$ , as determined by the criterion in Eq. (A6). Specifically:

- When  $\beta_0 > \gamma_0$  and  $\beta_0 < 0$ , all the boundary points are unsaturated (Subplot h. and i.).
- When  $\beta_0 > \gamma_0$  and  $\beta_0 > 0$ , only some of the boundary points are saturated (Subplot f. and g.).
- When  $\beta_0 < \gamma_0$  and  $\beta_0 > 0$ , only some of the boundary points are saturated (Subplot l. and m.).
- Finally, when  $\beta_0 < \gamma_0$  and  $\beta_0 < 0$ , no boundary point is saturated (Subplot j. and k.).

*Cyan zone:* In this region,  $\beta_0 < 0$ , while  $\alpha_0 + \gamma_0$ , may have either sign. If  $\alpha_0 + \gamma_0 > 0$  then Eq. (A6) requires  $p < 0$ , which lies outside the physical domain  $p \in [0, 1]$ . Hence, no saturated boundary point can exist in this case. If instead  $\alpha_0 + \gamma_0 < 0$ , then within the cyan region we have,  $\beta_0 < (\alpha_0 + \gamma_0)$ , and Eq. (A6) again cannot be satisfied. Thus, no saturated boundary point exists in this case either.

## Appendix B: Non-isolated fixed points at the intersection of surfaces— $n = 1$ and $F(p, q, n) = 0$

The eigenvalues of the Jacobian matrix at the replete state ( $n = 1$ ) are given by:

- (i)  $\lambda_1 = (1 - (p + q))$
- (ii)  $\lambda_2 = qA_1 + (1 - p)B_1$
- (iii)  $\lambda_3 = 0$

where,  $A_1 = q(\beta_1 - \gamma_1) + (1 - 2r)(\alpha_1 + \gamma_1) + \beta_1$ ,  $B_1 = (1 + r)(\beta_1 - \gamma_1) - A_1$ . The zero eigenvalue  $\lambda_3 = 0$  indicates neutral stability along the corresponding eigenvector.

Subplot (B) of Fig. (1) highlights the distinct stability regions associated with different underlying games. The existence and stability properties of the non-isolated fixed points and boundary points at the depleted state are analyzed in detail in the following subsection. Importantly, the fixed points and their stability at  $n = 1$  depend solely on the game played at the repleted state and are independent of the game played at  $n = 0$ .

### 1. Construction of Fig. 1(B)

The expressions for  $\lambda_2$  and for the fixed-point condition  $F(p, q, 1) = 0$ , at  $n = 1$  have exactly the same structure as their counterparts  $\lambda_2$  and  $F(p, q, 0) = 0$  at  $n = 0$ , except that with the parameters  $(\alpha_0, \beta_0, \gamma_0)$  replaced by  $(\alpha_1, \beta_1, \gamma_1)$ . Therefore, we conclude, from our earlier analysis, that whenever  $\beta_1 > \gamma_1$ , the sign of the eigenvalue  $\lambda_2$  is positive, and when  $\beta_1 < \gamma_1$ , then the sign of the eigenvalue  $\lambda_2$  is negative. The fixed-point curve retains the same qualitative structure as in the  $n = 0$  (see subplot (A) of Fig. 1), with the sole exception that  $\lambda_1$  becomes negative whenever  $p + q > 1$ .

However, the analysis of the saturated boundary points differs from the  $n = 0$  case. At  $n = 1$ , the only possible saturated boundary points lie on the boundary  $p = 1$  (see discussion in Section III). A saturated point on the boundary  $p = 1$  arises only when the generosity level  $q$  satisfies,

$$(\alpha_1 + \beta_1)(1 - q) > \gamma_1, \quad \forall q \in [0, 1]. \quad (\text{B1})$$

In the following discussion, we have analyzed the existence of saturated points for all relevant parameter values:

*Orange zone:* In this region,  $\alpha_1 + \beta_1 > \gamma_1$ . Since  $\gamma_1$  may be either positive or negative, the number of saturated points depends on the sign of  $\gamma_1$  as indicated by Eq. (B1). When  $\gamma_1 < 0$ , all the boundary points are saturated (see Subplot b.). In contrast, when  $\gamma_1 > 0$ , only a subset of the boundary points is saturated (see Subplot a.).

*Violet zone:* In the violet region,  $\alpha_1 + \beta_1 > \gamma_1$ . Therefore, according to Eq. (B1), the boundary  $p = 1$  is always saturated.

*Yellow zone:* In the yellow region, where  $\alpha_1 + \beta_1 < \gamma_1$ , and hence Eq. (B1) implies that no boundary point is saturated.

*Green zone:* In the green region, even though  $\alpha_1 + \beta_1 < \gamma_1$ , the behavior of the boundary  $p = 1$  depends on the sign of  $\gamma_1$ . When  $\gamma_1 > 0$ , no boundary point is saturated (see Subplot j.).

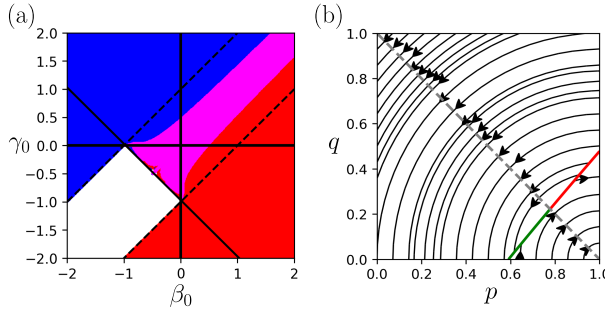


FIG. 5. Summary of the sign of the eigenvalue  $\lambda_2$ : Subplot (a) summarizes the sign of the eigenvalue  $\lambda_2$  in the  $\beta_0$ - $\gamma_0$  parameter plane for the fixed-point curve arising from the intersection of the surfaces  $n = 0$  and  $F(p, q, n) = 0$ . In this plot, blue and red colors indicate regions where  $\lambda_2$  is negative and positive, respectively. The magenta region denotes parameter values for which  $\lambda_2$  is negative along one portion of the fixed-point curve and positive along another portion. The white region represents parameter values for which no fixed-point curve exists. Subplot (b) corresponds to the magenta region and illustrates representative trajectories approaching or departing from the fixed-point curve, demonstrating that one portion of the curve is stable while the remaining portion is unstable.

In contrast, when  $\gamma_1 < 0$ , a subset of the boundary points becomes saturated (see Subplot e.).

*Pink zone:* In the pink region,  $\beta_1$  may be either greater or less than  $\gamma_1$ . Although this region satisfies  $\alpha_1 + \beta_1 > \gamma_1$ , the parameter  $\gamma_1$  itself may take either positive or negative values. From Eq. (B1), it follows that  $\gamma_1 < 0$ , all boundary points are saturated. In contrast, when  $\gamma_1 > 0$ , only a subset of the boundary points becomes saturated.

*Cyan zone:* Since  $\alpha_1 + \beta_1 > \gamma_1$  in this region, and both  $\gamma_1$  and  $\alpha_1 + \beta_1$  are negative, Eq. (B1) implies that all boundary points on  $p = 1$  are saturated.

#### Appendix C: Non-isolated fixed points at the intersection of surfaces— $p + q = 1$ and $F(p, q, n) = 0$

The eigenvalues of the Jacobian matrix at the intermediate state of resource  $n \in (0, 1)$  are given by:

$$(i) \lambda_1 + \lambda_2 = \frac{2pq}{(1-r)^2(1-r^2)} [(1-n)(\beta_0 - \gamma_0) + n(\beta_1 - \gamma_1)]$$

$$(ii) \lambda_1 \lambda_2 = \frac{n(1-n)}{4pq} [(\beta_1 + \gamma_1 + 2\alpha_1 - \beta_0 - \gamma_0 - 2\alpha_0)q - (\alpha_1 - \alpha_0)]$$

$$(iii) \lambda_3 = 0$$

Using Eq. (C3) for the internal fixed points, we ultimately get,

$$\lambda_1 \lambda_2 = \frac{n(1-n)}{4pq} \frac{(\beta_1 + \gamma_1)\alpha_0 - (\beta_0 + \gamma_0)\alpha_1}{(1-n)(\beta_0 + \gamma_0 + 2\alpha_0) + n(\beta_1 + \gamma_1 + 2\alpha_1)}. \quad (C1)$$

For a fixed point to be stable, the sum of the relevant eigenvalues must be negative  $\lambda_1 + \lambda_2 < 0$  and their product must be positive  $\lambda_1 \lambda_2 > 0$  [101]. Thus, the stability of the internal

fixed points depends on the games played at both  $n = 0$  and  $n = 1$ .

Subplot (C) of Fig. (1) illustrates the corresponding stability regions: where in parameter space of  $\beta_1 + \gamma_1$  vs  $\beta_0 + \gamma_0$  the fixed point stability structure has been shown in subsubplots *a*. and *b*. for violate region and olive region respectively.

#### 1. Construction of Fig. 1(C)

It illustrates the existence and stability properties of the internal fixed points, defined by the conditions  $p + q = 1$  and  $F(p, q, n) = 0$ . The fixed-point curve follows

$$F(p, n) = (1-n)[(\beta_0 - \gamma_0)p + (\alpha_0 + \gamma_0)(2p - 1) - \beta_0] + n[(\beta_1 - \gamma_1)p + (\alpha_1 + \gamma_1)(2p - 1) - \beta_1] = 0, \quad (C2)$$

which implies

$$q = \frac{(1-n)\alpha_0 + n\alpha_1}{(1-n)(\beta_0 + \gamma_0 + 2\alpha_0) + n(\beta_1 + \gamma_1 + 2\alpha_1)}. \quad (C3)$$

Note that for our system  $\alpha_0, \alpha_1 > 0$  always, so the necessary condition for existence of the fixed point is  $(1-n)(\beta_0 + \gamma_0 + 2\alpha_0) + n(\beta_1 + \gamma_1 + 2\alpha_1) > 0$ , which implies:

$$n > \frac{\beta_0 + \gamma_0 + 2\alpha_0}{(\beta_1 + \gamma_1 + 2\alpha_1) - (\beta_0 + \gamma_0 + 2\alpha_0)} \quad (C4)$$

whenever,  $\beta_1 + \gamma_1 + 2\alpha_1 > \beta_0 + \gamma_0 + 2\alpha_0$ . From Eq. (C2), we observe that the fixed-point curve intersects the  $n = 0$  plane at

$$p = \frac{(\alpha_0 + \beta_0 + \gamma_0)}{\alpha_0 + (\alpha_0 + \beta_0 + \gamma_0)}, \quad (C5)$$

Similarly, the fixed-point curve intersects the  $n = 1$  plane at

$$p = \frac{(\alpha_1 + \beta_1 + \gamma_1)}{\alpha_1 + (\alpha_1 + \beta_1 + \gamma_1)}. \quad (C6)$$

In addition, the curve intersects the plane  $p = 0$  at

$$n_m = \frac{-(\alpha_0 + \beta_0 + \gamma_0)}{(\alpha_1 + \beta_1 + \gamma_1) - (\alpha_0 + \beta_0 + \gamma_0)}, \quad (C7)$$

and does not intersect the plane  $p = 1$ . Just from the eigenvalue expressions—*(i)*, *(ii)*, we can directly draw the following conclusions: Whenever  $(\beta_1 + \gamma_1)\alpha_0 < (\beta_0 + \gamma_0)\alpha_1$ , then the product of the eigenvalues  $\lambda_1 \lambda_2 < 0$  (see Eq. (C1)), since the denominator in Eq. (C1) is always positive whenever the fixed point line Eq. (C3) exists. Therefore, the corresponding fixed points are saddles. On the other hand, whenever  $(\beta_1 + \gamma_1)\alpha_0 > (\beta_0 + \gamma_0)\alpha_1$  the eigenvalue product  $\lambda_1 \lambda_2 > 0$ , which implies the fixed point can be stable or unstable depending on the sign of  $\lambda_1 + \lambda_2$  and hence the sign and relative values of  $\beta_1 - \gamma_1$  and  $\beta_0 - \gamma_0$ . We now examine these conditions in detail to clarify the existence and stability of internal fixed points across different parameter regimes.

*Grey zone:* In this parameter region  $(\beta_1 + \gamma_1)\alpha_0 < (\beta_0 + \gamma_0)\alpha_1$ , implies that the eigenvalues  $\lambda_1$  and  $\lambda_2$  have opposite

signs. Consequently, the system possesses saddle fixed points. *Olive zone:* In this parameter regime, the condition  $(\beta_1 + \gamma_1)\alpha_0 > (\beta_0 + \gamma_0)\alpha_1$  ensures that  $\lambda_1\lambda_2 > 0$ , so the two eigenvalues share the same sign. Moreover, in this region both  $(\beta_1 + \gamma_1) > 0$  (0, as our assumption, its corresponds to defections dominant game parameters) and  $(\beta_0 + \gamma_0) > -\alpha_0$ , consequently from Eq. (C5) and (C6), the fixed-point curve intersects both the  $n = 0$  and  $n = 1$  plane. To determine the stability of the fixed points—that is, the sign of  $\lambda_1 + \lambda_2$ —we must analyze the relative signs of  $(\beta_0 - \gamma_0)$  and  $(\beta_1 - \gamma_1)$ . Since  $\lambda_1 + \lambda_2$  is a linear and monotonic function of  $n$ , the stability of the entire fixed-point curve can be inferred solely from its behaviour at the two endpoints,  $n = 0$  and  $n = 1$ . Accordingly, in the first quadrant, the fixed points are always unstable, whereas in the third quadrant, they are always stable. In contrast, in the second and fourth quadrants, the stability behaviour differs between the two endpoints; thus, in these regions, part of the fixed-point curve is stable while the remaining part is unstable.

*Violet zone:* In this parameter regime  $(\beta_0 + \gamma_0) < -\alpha_0$  and  $(\beta_1 + \gamma_1) > 0$ , we have  $\lambda_1\lambda_2 > 0$ . Furthermore, from Eq. (C5), (C6), and (C7), the fixed-point curve is seen to intersect both the  $n = 1$  plane and the  $p = 0$  plane. To determine the stability of these fixed points—that is, the sign of  $\lambda_1 + \lambda_2$ —we must examine the relative signs of  $(\beta_0 - \gamma_0)$  and  $(\beta_1 - \gamma_1)$ , as summarized in subplot *a.* of Fig. (1). In the first quadrant of Subplot *a.*, where  $(\beta_0 - \gamma_0) > 0$  and  $(\beta_1 - \gamma_1) > 0$ , we have  $\lambda_1 + \lambda_2 > 0$  and the fixed points are unstable. In contrast, in the third quadrant of Subplot *a.*, where  $(\beta_0 - \gamma_0) < 0$  and  $(\beta_1 - \gamma_1) < 0$ , which obtain  $\lambda_1 + \lambda_2 < 0$ , and the fixed points are stable. In the second quadrant of Subplot *a.*, the condition  $(\beta_1 - \gamma_1) > 0$ , implies that the fixed point lying on the  $n = 1$  plane is always unstable. The stability of the fixed point on the  $p = 0$  plane, however, depends on the value of  $n$  at that fixed point. Substituting  $n = n_m$  into the expression for  $\lambda_1 + \lambda_2$ , one finds that the sign of  $\lambda_1 + \lambda_2$  is determined by the sign of  $(\alpha_1 + \beta_1 + \gamma_1)(\beta_0 - \gamma_0) - (\alpha_0 + \beta_0 + \gamma_0)(\beta_1 - \gamma_1)$ . Hence, the fixed point is unstable whenever

$$(\beta_0 - \gamma_0) > -K, \quad (C8)$$

and stable whenever

$$(\beta_0 - \gamma_0) < -K, \quad (C9)$$

where  $K = |A|(\beta_1 - \gamma_1)/|B|$ ,  $A = \alpha_0 + \beta_0 + \gamma_0$  and  $B = \alpha_1 + \beta_1 + \gamma_1$ . We therefore conclude that in the second quadrant the fixed-point curve is entirely unstable when condition (C8) is hold; otherwise, only part of the curve is unstable. Similarly, in the fourth quadrant, the fixed-point curve is completely stable whenever condition (C9) is satisfied; otherwise, only a portion of it is stable.

#### Appendix D: Analysis for Constructing Subplots (b) and (c) in Fig. 3

Based on the generic analysis presented in Appendix C, we now examine its physical interpretation in terms of reward and punishment mechanisms under different resource

states. Specifically, we consider reward ( $\rho_0^+$ ) and punishment ( $\rho_0^-$ ) at the depleted resource state, and reward ( $\rho_1^+$ ) and punishment ( $\rho_1^-$ ) at the replete resource state. These are analyzed within the framework of donation games, characterized by benefits  $b_0$  and  $b_1$  at the depleted and replete resource states, respectively, and a cost  $c$ . The generic symbolic parameters introduced in the analytical treatment correspond to the following physical quantities:  $\beta_0 = c - \rho_0^+$ ,  $\beta_1 = c - \rho_1^+$ ,  $\gamma_0 = c - \rho_0^-$ ,  $\gamma_1 = c - \rho_1^-$ ,  $\alpha_0 = b_0 - c$  and  $\alpha_1 = b_1 - c$ .

We impose a predefined assumption that individual behavior is defection-dominated when the resource state is replete. Consequently, both  $\beta_1 > 0$  and  $\gamma_1 > 0$  hold. Under these conditions, we construct the corresponding dynamical outcomes shown in Fig. 3.

In this figure, the gray region is bounded by the condition  $\rho_0^+ + \rho_0^- < 2c - \frac{\alpha_0}{\alpha_1}(2c - \rho_1^+ - \rho_1^-)$ ; and represents the saddle fixed-point curve region of the  $(\rho_0^+, \rho_0^-)$  parameter space, which is indicated by the chain-dotted line. The complementary regime,  $\rho_0^+ + \rho_0^- > 2c - \frac{\alpha_0}{\alpha_1}(2c - \rho_1^+ - \rho_1^-)$ , admits the possibility of either stable or unstable continuum of fixed points. Within this regime, we further distinguish two sub-cases depending on whether  $\rho_0^+ + \rho_0^- < b_0 + c$  or  $\rho_0^+ + \rho_0^- > b_0 + c$ ; which are separated by the dotted black line in the parameter space.

(a)  $\rho_0^+ + \rho_0^- > 2c - \frac{\alpha_0}{\alpha_1}(2c - \rho_1^+ - \rho_1^-)$  and  $\rho_0^+ + \rho_0^- > b_0 + c$ : By expressing the generic coefficients  $(\beta_0, \gamma_0, \beta_1, \gamma_1)$  in terms of reward and punishment parameters, Panel (a) of subplot (C) in Fig. 1, corresponding to the intermediate resource state  $n \in (0, 1)$ , reveals the associated stability regions, which are shown in Fig. 3. Here, the stability of the fixed-point curve depends on the relative magnitudes and signs of  $(\rho_0^- - \rho_0^+)$  and  $(\rho_1^- - \rho_1^+)$ , as discussed below.

When  $\rho_1^- - \rho_1^+ > 0$ , for  $(\rho_0^- - \rho_0^+) > -K$ , the fixed-point curve is unstable, and for  $(\rho_0^- - \rho_0^+) < -K$ , part of the fixed-point curve is stable, while the remaining part is unstable, where  $K = -\frac{|b_0 + c - \rho_0^+ - \rho_0^-|}{b_1 + c - \rho_1^+ - \rho_1^-}(\rho_1^+ - \rho_1^-)$ .

On the other hand, Whenever  $(\rho_1^- - \rho_1^+) < 0$ , for  $(\rho_1^- - \rho_1^+) < K$ , the fixed-point curve is stable, and for  $(\rho_1^- - \rho_1^+) > K$ , part of the fixed-point curve is stable, while the remaining part is unstable.

(b)  $\rho_0^+ + \rho_0^- > 2c - \frac{\alpha_0}{\alpha_1}(2c - \rho_1^+ - \rho_1^-)$  and  $\rho_0^+ + \rho_0^- < b_0 + c$ : By expressing the generic coefficients  $(\beta_0, \gamma_0, \beta_1, \gamma_1)$  in terms of reward and punishment parameters, Panel (b) of subplot (C) in Fig. 1, corresponding to the intermediate resource state  $n \in (0, 1)$ , reveals the associated stability regions, which are shown in Fig. 3. Here, the stability of the fixed-point curve depends on the relative magnitudes and signs of  $(\rho_0^- - \rho_0^+)$  and  $(\rho_1^- - \rho_1^+)$ , as discussed below.

When  $(\rho_1^- - \rho_1^+) > 0$  the corresponding fixed point at  $n = 1$  is unstable. Now if  $(\rho_0^- - \rho_0^+) > 0$ , the  $\lambda_1 + \lambda_2 < 0$  for any allowed values of  $n$  (see Appendix C) and hence the whole fixed-point curve is unstable, and if

$(\rho_0^- - \rho_0^+) < 0$ , the part of the fixed-point curve is stable and the remaining is unstable depending on the relative values of  $(\rho_0^- - \rho_0^+)$  and  $(\rho_1^- - \rho_1^+)$ . On the other hand, when  $(\rho_1^- - \rho_1^+) < 0$  the corresponding fixed-point curve at  $n = 1$  is stable. Now, If  $(\rho_0^- - \rho_0^+) < 0$ , the  $\lambda_1 + \lambda_2 < 0$  (see Appendix C) for any allowed values of  $n$ , therefore, the whole fixed-point curve is sta-

ble. On the other hand, if  $(\rho_0^- - \rho_0^+) > 0$ , the part of the fixed-point curve is stable and the remaining is unstable depending on the relative values of  $(\rho_0^- - \rho_0^+)$  and  $(\rho_1^- - \rho_1^+)$ .

---

[1] G. Hardin, *Science* **162**, 1243 (1968).

[2] D. J. Rankin, K. Bargum, and H. Kokko, *Trends in Ecology & Evolution* **22**, 643–651 (2007).

[3] B. M. Frischmann, A. Marciano, and G. B. Ramello, *Journal of Economic Perspectives* **33**, 211–228 (2019).

[4] M. A. Janssen, S. Smith-Heisters, R. Aggarwal, and M. L. Schoon, *Environmental Education Research* **25**, 1587–1604 (2019).

[5] E. Ostrom, “Tragedy of the commons,” in *The New Palgrave Dictionary of Economics* (Palgrave Macmillan UK, 2008) p. 1–5.

[6] D. W. Bromley and M. M. Cernea, *The management of common property natural resources: Some conceptual and operational fallacies*, Vol. 57 (World Bank Publications, 1989).

[7] E. Zea-Cabrera, Y. Iwasa, S. Levin, and I. Rodríguez-Iturbe, *Water Resources Research* **42** (2006), 10.1029/2005wr004514.

[8] R. Lal, “Tragedy of the global commons: Soil, water and air,” in *Climate Change, Intercropping, Pest Control and Beneficial Microorganisms* (Springer Netherlands, 2009) p. 9–11.

[9] I. A. Shiklomanov, *Water International* **25**, 11–32 (2000).

[10] M. Fraser, *Eos, Transactions American Geophysical Union* **84**, 332–332 (2003).

[11] E. Ostrom, *Annual review of political science* **2**, 493 (1999).

[12] S. F. Pires and W. D. Moreto, *European Journal on Criminal Policy and Research* **17**, 101 (2011).

[13] B. H. Pandit and G. B. Thapa, *Environmental conservation* **30**, 283 (2003).

[14] D. S. Falster and M. Westoby, *Trends in Ecology & Evolution* **18**, 337–343 (2003).

[15] M. A. Nowak and K. Sigmund, *Nature* **393**, 573–577 (1998).

[16] P. LaPorte, C. Hilbe, and M. A. Nowak, *PLOS Computational Biology* **19**, e1010987 (2023).

[17] M. A. Nowak, *Science* **314**, 1560 (2006).

[18] R. L. Trivers, *The Quarterly Review of Biology* **46**, 35–57 (1971).

[19] R. Axelrod and W. D. Hamilton, *Science* **211**, 1390–1396 (1981).

[20] C. Hilbe, K. Chatterjee, and M. A. Nowak, *Nature Human Behaviour* **2**, 523–523 (2018).

[21] J. García and M. van Veelen, *Frontiers in Robotics and AI* **5** (2018), 10.3389/frobt.2018.00102.

[22] J. M. Smith, *Evolution and the Theory of Games* (Cambridge University Press, 1982).

[23] M. A. NOWAK, *Evolutionary Dynamics: Exploring the Equations of Life* (Harvard University Press, 2006).

[24] J. M. SMITH and G. R. PRICE, *Nature* **246**, 15–18 (1973).

[25] J. Hofbauer and K. Sigmund, *Evolutionary Games and Population Dynamics* (Cambridge University Press, 1998).

[26] A. Melbinger and M. Vergassola, *Scientific Reports* **5** (2015), 10.1038/srep15211.

[27] A. Sih, M. C. O. Ferrari, and D. J. Harris, *Evolutionary Applications* **4**, 367–387 (2011).

[28] R. Levins, *Evolution in Changing Environments* (Princeton University Press, Princeton, 1968).

[29] H. B. D. Kettlewell, *Heredity* **9**, 323–342 (1955).

[30] J. S. Brown and B. P. Kotler, *Ecology Letters* **7**, 999–1014 (2004).

[31] L. Muscatine and J. W. Porter, *BioScience* **27**, 454–460 (1977).

[32] P. Avila and C. Mullon, *Philosophical Transactions of the Royal Society B* **378** (2023), 10.1098/rstb.2021.0502.

[33] M. Doebeli, *Adaptive Diversification (MPB-48)* (Princeton University Press, 2011).

[34] R. E. Lenski, *The ISME Journal* **11**, 2181–2194 (2017).

[35] J. R. Meyer, D. T. Dobias, S. J. Medina, L. Servilio, A. Gupta, and R. E. Lenski, *Science* **354**, 1301–1304 (2016).

[36] D. S. Robertson, *Journal of Theoretical Biology* **152**, 469–484 (1991).

[37] D. M. Post and E. P. Palkovacs, *Philosophical Transactions of the Royal Society B: Biological Sciences* **364**, 1629–1640 (2009).

[38] T. Killingback, M. Doebeli, and C. Hauert, *Biological Theory* **5**, 3–6 (2010).

[39] D. Passagem-Santos and L. Perfeito, (2018), 10.1101/464362.

[40] J. S. McKinnon and H. D. Rundle, *Trends in Ecology & Evolution* **17**, 480–488 (2002).

[41] T. Yoshida, L. E. Jones, S. P. Ellner, G. F. Fussmann, and N. G. Hairston, *Nature* **424**, 303–306 (2003).

[42] J. L. Brooks and S. I. Dodson, *Science* **150**, 28–35 (1965).

[43] E. P. Palkovacs and D. M. Post, *Evolutionary Ecology Research* **10**, 699 (2008).

[44] D. M. Post, E. P. Palkovacs, E. G. Schielke, and S. I. Dodson, *Ecology* **89**, 2019–2032 (2008).

[45] D. N. Reznick, F. H. Shaw, F. H. Rodd, and R. G. Shaw, *Science* **275**, 1934–1937 (1997).

[46] E. P. Palkovacs and D. M. Post, *Ecology* **90**, 300–305 (2009).

[47] P. R. Grant, *Ecology and Evolution of Darwin’s Finches (Princeton Science Library Edition)* (Princeton University Press, 1986).

[48] N. G. Hairston, S. P. Ellner, M. A. Geber, T. Yoshida, and J. A. Fox, *Ecology Letters* **8**, 1114–1127 (2005).

[49] P. R. Grant and B. R. Grant, *Science* **313**, 224–226 (2006).

[50] T. G. Whitham, J. K. Bailey, J. A. Schweitzer, S. M. Shuster, R. K. Bangert, C. J. LeRoy, E. V. Lonsdorf, G. J. Allan, S. P. DiFazio, B. M. Potts, D. G. Fischer, C. A. Gehring, R. L. Lindroth, J. C. Marks, S. C. Hart, G. M. Wimp, and S. C. Wooley, *Nature Reviews Genetics* **7**, 510–523 (2006).

[51] J. S. Weitz, C. Eksin, K. Paarporn, S. P. Brown, and W. C. Ratcliff, *Proc. Natl. Acad. Sci. U.S.A.* **113**, E7518 (2016).

[52] Y.-H. Lin and J. S. Weitz, *Physical Review Letters* **122** (2019), 10.1103/physrevlett.122.148102.

[53] A. R. Tilman, J. B. Plotkin, and E. Akçay, *Nature Communications* **11** (2020), 10.1038/s41467-020-14531-6.

[54] J. D. Bairagya, S. S. Mondal, D. Chowdhury, and S. Chakraborty, *Physical Review E* **104** (2021), 10.1103/physreve.104.044407.

[55] S. S. Mondal, M. Pathak, and S. Chakraborty, *Journal of Physics: Complexity* **3**, 025005 (2022).

[56] J. D. Bairagya, S. S. Mondal, D. Chowdhury, and S. Chakraborty, *Journal of Physics: Complexity* **4**, 025002 (2023).

[57] S. Sohel Mondal, A. Ray, and S. Chakraborty, *Chaos: An Interdisciplinary Journal of Nonlinear Science* **34** (2024), 10.1063/5.0190800.

[58] A. Mandal, S. Sarkar, S. Chakraborty, and P. S. Dutta, *Proceedings of the Royal Society A: Mathematical, Physical and Engineering Sciences* **481** (2025), 10.1098/rspa.2024.0915.

[59] P. D. Taylor and L. B. Jonker, *Mathematical Biosciences* **40**, 145–156 (1978).

[60] P. Schuster and K. Sigmund, *Journal of Theoretical Biology* **100**, 533–538 (1983).

[61] P. Schuster and K. Sigmund, *Berichte der Bunsengesellschaft für physikalische Chemie* **89**, 668–682 (1985).

[62] K. M. Page and M. A. Nowak, *Journal of Theoretical Biology* **219**, 93–98 (2002).

[63] R. Cressman, *Evolutionary Dynamics and Extensive Form Games*, 1st ed., MIT Press Books, Vol. 1 (The MIT Press, Cambridge, MA, 2003).

[64] L. A. Martinez-Vaquero, J. A. Cuesta, and A. Sánchez, *PLoS ONE* **7**, e35135 (2012).

[65] D. Fudenberg and E. Maskin, *The American Economic Review* **80**, 274 (1990).

[66] M. A. Nowak and K. Sigmund, *Science* **303**, 793–799 (2004).

[67] S. A. H. Geritz, J. A. J. Metz, K. Kisdi, and G. Meszéna, *Physical Review Letters* **78**, 2024–2027 (1997).

[68] S. Geritz, E. Kisdi, G. Meszena, and J. Metz, *Evolutionary Ecology* **12**, 35–57 (1998).

[69] F. Diercole and S. Rinaldi, *Analysis of Evolutionary Processes: The Adaptive Dynamics Approach and Its Applications: The Adaptive Dynamics Approach and Its Applications* (Princeton University Press, 2008).

[70] K. Kisdi and S. A. H. Geritz, *Journal of Mathematical Biology* **61**, 165–169 (2009).

[71] R. Bshary and A. S. Grutter, *Biology Letters* **1**, 396–399 (2005).

[72] E. T. Kiers, R. A. Rousseau, S. A. West, and R. F. Denison, *Nature* **425**, 78–81 (2003).

[73] E. T. Kiers, M. Duhamel, Y. Beesetty, J. A. Mensah, O. Franken, E. Verbruggen, C. R. Fellbaum, G. A. Kowalchuk, M. M. Hart, A. Bago, T. M. Palmer, S. A. West, P. Vandenoornhuyse, J. Jansa, and H. Bücking, *Science* **333**, 880–882 (2011).

[74] E. Fehr and S. Gächter, *Nature* **415**, 137–140 (2002).

[75] R. Boyd, H. Gintis, S. Bowles, and P. J. Richerson, *Proceedings of the National Academy of Sciences* **100**, 3531–3535 (2003).

[76] S. Bowles and H. Gintis, *A Cooperative Species: Human Reciprocity and Its Evolution* (Princeton University Press, 2011).

[77] T. Kiyonari and P. Barclay, *Journal of Personality and Social Psychology* **95**, 826–842 (2008).

[78] C. Hauert, *Journal of Theoretical Biology* **267**, 22–28 (2010).

[79] J. Stoop, D. van Soest, and J. Vyrastekova, *Journal of Environmental Economics and Management* **88**, 300–310 (2018).

[80] T. H. Clutton-Brock and G. A. Parker, *Nature* **373**, 209–216 (1995).

[81] T. Sasaki and S. Uchida, *Proceedings of the Royal Society B: Biological Sciences* **280**, 20122498 (2013).

[82] S. Johnson, *Royal Society Open Science* **2**, 150223 (2015).

[83] G. W. Greenwood, in *2016 IEEE Conference on Computational Intelligence and Games (CIG)* (IEEE, 2016) p. 1–7.

[84] X. Chen and A. Szolnoki, *PLOS Computational Biology* **14**, e1006347 (2018).

[85] K. Sigmund, C. Hauert, and M. A. Nowak, *Proceedings of the National Academy of Sciences* **98**, 10757–10762 (2001).

[86] *Reward and Punishment in Social Dilemmas* (Oxford University Press, 2014).

[87] A. R. Góis, F. P. Santos, J. M. Pacheco, and F. C. Santos, *Scientific Reports* **9** (2019), 10.1038/s41598-019-52524-8.

[88] J. Liu, M. Li, M. Alam, Y. Chen, and T. Wu, *Mobile Networks and Applications* **24**, 1279–1294 (2019).

[89] Y. Fang, T. P. Benko, M. Perc, H. Xu, and Q. Tan, *Proceedings of the Royal Society A: Mathematical, Physical and Engineering Sciences* **475**, 20190349 (2019).

[90] H. Ozono, Y. Kamijo, and K. Shimizu, *Scientific Reports* **10** (2020), 10.1038/s41598-020-64930-4.

[91] M. Nowak and K. Sigmund, *Acta Applicandae Mathematicae* **20**, 247 (1990).

[92] M. Nowak and K. Sigmund, *Journal of Theoretical Biology* **137**, 21–26 (1989).

[93] J. Hofbauer and K. Sigmund, *Applied Mathematics Letters* **3**, 75–79 (1990).

[94] U. Dieckmann and R. Law, *Journal of Mathematical Biology* **34**, 579 (1996).

[95] J. Metz, R. Nisbet, and S. Geritz, *Trends Ecol. Evol.* **7**, 198 (1992).

[96] J. E. Marsden and M. McCracken, *The Hopf Bifurcation and Its Applications* (Springer New York, 1976).

[97] K. Sigmund, *The Calculus of Selfishness* (Princeton University Press, Princeton, 2010).

[98] M. A. Nowak and K. Sigmund, *Nature* **437**, 1291–1298 (2005).

[99] A. McAvoy and C. Hauert, *Theoretical Population Biology* **113**, 13–22 (2017).

[100] I. Kareva, B. Morin, and G. Karev, *Bulletin of mathematical biology* **75**, 565 (2013).

[101] S. H. Strogatz, “Nonlinear dynamics and chaos: With applications to physics, biology, chemistry, and engineering (studies in nonlinearity),” (Westview Press, 2014).